POMC neurons control fertility through differential signaling of MC4R in Kisspeptin neurons

Authors:
Rajae Talbi[1,2*], Todd L. Stincic[4,8*], Kaitlin Ferrari[2], Choi Ji Hae[2], Karol Walec[2], Elizabeth Medve[2], Achi Gerutshang[2], Silvia León[1,2], Elizabeth A. McCarthy[1,2], Oline K. Rønnekleiv[3,4], Martin J. Kelly[3,4,6] and Víctor M. Navarro[1,2,5,6]

[1]Harvard Medical School, Boston, MA, USA; [2]Division of Endocrinology, Diabetes and Hypertension, Department of Medicine, Brigham and Women's Hospital, Boston, MA, USA; [3]Department of Chemical Physiology and Biochemistry, Oregon Health & Science University, Portland, OR, USA; [4]Division of Neuroscience, Oregon National Primate Research Center, Beaverton, OR, USA; [5]Harvard Program in Neuroscience, Boston, MA, USA

*These authors contributed equally
[6] Corresponding authors
[8]Present address: Department of Biology, Appalachian State University, Boone, NC 28608.

Correspondence:
Victor M. Navarro, PhD, Division of Endocrinology, Diabetes and Hypertension, Department of Medicine, Brigham and Women's Hospital and Harvard Medical School, 221 Longwood Avenue, Room 219, Boston, Massachusetts 02115. E-mail: vnavarro@bwh.harvard.edu.

Martin J. Kelly, PhD, Department of Chemical Physiology and Biochemistry, Oregon Health & Science University, 3181 SW Sam Jackson Park Road, Portland, OR 97239. E-mail: kellym@ohsu.edu .

Keywords:
Kiss1 neurons, POMC neurons, MC4R, Fertility, Ovulation, Obesity, Estradiol.

Abstract

Inactivating mutations in the melanocortin 4 receptor (*MC4R*) gene cause monogenic obesity. Interestingly, female patients also display various degrees of reproductive disorders, in line with the subfertile phenotype of MC4RKO female mice. However, the cellular mechanisms by which MC4R regulates reproduction are unknown. Kiss1 neurons directly stimulate gonadotropin-releasing hormone (GnRH) release through two distinct populations; the Kiss1^{ARH} neurons, controlling GnRH pulses, and the sexually dimorphic Kiss1$^{AVPV/PeN}$ neurons controlling the preovulatory LH surge. Here, we show that *Mc4r* expressed in Kiss1 neurons regulates fertility in females. *In vivo*, deletion of *Mc4r* from Kiss1 neurons in female mice replicates the reproductive impairments of MC4RKO mice without inducing obesity. Conversely, reinsertion of *Mc4r* in Kiss1 neurons of MC4R null mice restores estrous cyclicity and LH pulsatility without reducing their obese phenotype. *In vitro*, we dissect the specific action of MC4R on Kiss1^{ARH} vs Kiss1$^{AVPV/PeN}$ neurons and show that MC4R activation excites Kiss1^{ARH} neurons through direct synaptic actions. In contrast, Kiss1$^{AVPV/PeN}$ neurons are normally inhibited by MC4R activation except under elevated estradiol levels, thus facilitating the activation of Kiss1$^{AVPV/PeN}$ neurons to induce the LH surge driving ovulation in females. Our findings demonstrate that POMC^{ARH} neurons acting through MC4R, directly regulate reproductive function in females by stimulating the “pulse generator” activity of Kiss1^{ARH} neurons and restricting the activation of Kiss1$^{AVPV/PeN}$ neurons to the time of the estradiol-dependent LH surge, and thus unveil a novel pathway of the metabolic regulation of fertility by the melanocortin system.

Introduction

Obesity rates have skyrocketed in Western societies in the last decades, resulting in an alarming rise in comorbidities that place a significant burden on healthcare systems. The increase in obesity correlates with a decrease in fertility rates, leading to conception challenges that are experienced by approximately 15% of couples in the United States currently (1).

The melanocortin 4 receptor (MC4R) binds i) α-melanocyte stimulating hormone (αMSH), an agonist product of the pro-opiomelanocortin (*Pomc*) gene, and ii) the inverse agonist, agouti-related peptide (AgRP), to regulate food intake and energy expenditure (2, 3). While the role of MC4R on food intake is largely mediated by neurons located in the paraventricular nucleus of the hypothalamus (PVN) (4), its expression in the brain is widespread (5) with the specific function of the different MC4R-expressing neurons in areas beyond the PVN remaining to be fully explored. Inactivating mutations in *MC4R* are a leading cause of monogenic obesity in humans (6) and cause excessive obesity and hyperphagia in mice (7). Scant evidence in humans shows an association between *MC4R* mutations and higher incidence of hypogonadotropic hypogonadism (HH) (8), alterations in the timing of puberty onset (9), and polycystic ovary syndrome (PCOS) (10); however, other studies have shown no association between MC4R and reproductive disorders (6). Therefore, the role of MC4R signaling in reproductive function in humans remains controversial despite the clear association found in mice. Supporting this role of MC4R, *Mc4r* null mice display an array of reproductive abnormalities that largely affects females, characterized by irregular estrous cycles, disrupted luteinizing hormone (LH) secretion, reduced corpora lutea and reduced fertility (11-13). Further evidence from mice demonstrates that MC4R agonists robustly increase LH release in a kisspeptin-dependent manner (14).

Kisspeptin is the most potent gonadotropin releasing hormone (GnRH) secretagogue known to date and it is mainly produced in two distinct neuronal populations. Kiss1 neurons of the arcuate

nucleus of the hypothalamus (Kiss1^{ARH}), present in both sexes, control the pulsatile (tonic) release of GnRH, and sex steroids attenuate their release of kisspeptin. Kiss1 neurons of the anteroventral periventricular continuum area (Kiss1$^{AVPV/PeN}$), are predominantly present in females, and are responsible for generating the preovulatory GnRH/LH surge essential for ovulation (15). Despite these critical roles of both populations of Kiss1 neurons for reproduction, the underlying mechanisms that determine how each Kiss1 population responds differently to sex steroids to regulate the GnRH tonic vs surge release remains unresolved.

In rodents, compelling evidence indicates a close interaction between Kiss1 neurons and the melanocortin system: 1) fibers from POMC neurons in the arcuate nucleus (POMC^{ARH}) project to and juxtapose Kiss1^{ARH} neurons (14); 2) the melanocortin signaling through MC4R contributes to the permissive role of leptin on puberty onset (14, 16, 17); and 3) MC4R expression on both Kiss1^{ARH} (18-20) and Kiss1$^{AVPV/PeN}$ (18, 21). Altogether, this evidence suggests a clear role for MC4R in Kiss1 neurons, in the control of reproductive maturation and fertility.

In this study, we investigated the contribution of MC4R signaling versus obesity *per se* in the etiology of the reproductive impairments observed in *Mc4r* null mice, which could explain similar impairments observed in humans. Using genetic mouse models with specific deletion or reinsertion of *Mc4r* in Kiss1 neurons, we show that MC4R action in Kiss1 neurons is necessary for normal reproductive function in female mice. Whole cell voltage clamp recordings evidenced an excitatory action of MC4R on Kiss1^{ARH} neurons and an estradiol-dependent inhibitory action on Kiss1$^{AVPV/PeN}$ neurons, with important implications for the timing of the preovulatory LH surge.

Results

Mc4r within Kiss1 neurons determines the timing of puberty onset in females.

The expression of *Mc4r* within Kiss1^{ARH} and Kiss1$^{AVPV/PeN}$ neurons has already been described elsewhere (18-21), suggesting a role for MC4R in the regulation of fertility. To further investigate

the specific role of MC4R in Kiss1 neurons, we generated a Kiss1-specific MC4R knockout mouse model (Kiss1-MC4RKO). The specific deletion of *Mc4r* from Kiss1 neurons, as well as the absence of global recombination, were confirmed through RNAscope. While Kiss1 neurons of Kiss1-MC4RKO mice lack *Mc4r* transcript compared to their control littermates (**Figure S*1A***), *Mc4r* was detectable in the PVN of all mice, which is a major site of *Mc4r* expression in the brain in the regulation of metabolism, therefore supporting the specific deletion of *Mc4r* only within Kiss1 neurons (**Figure S*1B***).

Puberty onset was assessed daily from weaning age through the monitoring of vaginal opening (VO) and first estrus (FE). Kiss1-MC4RKO females showed a significant advancement in the age of VO (P=0.0150, Kiss1-MC4RKO: 24.67± 0.39 vs controls: 26.32±0.53) and FE (P=0.0341, Kiss1-MC4RKO: 32.63±1.4 vs controls: 37.84±1.90) compared to their littermate controls (**Figure 1*A, B***). Body weight of Kiss1-MC4RKO females at the age of puberty onset was similar between groups (P=0.2596, Kiss1-MC4RKO: 12.41±0.30 vs controls: 12.89±0.26) (**Figure 1*C***). These data suggest that melanocortin signaling on Kiss1 neurons participates in the timing of puberty onset in females. Since the role of the melanocortin system on puberty onset is largely unexplored, we evaluated the expression profile of the main components of this system in the hypothalami of WT female mice at postnatal days (PND) 10, 15, 22 and 30. Interestingly, expressions of *Agrp*, *Mc3r* and *Mc4r* were significantly lower at the time of puberty onset (PND30) compared to earlier developmental ages (**Figure 1*D***). This supports our *in vivo* data and suggests that a decrease in the hypothalamic melanocortin signaling drives puberty onset, in line with the advancement in the age of VO and FE observed in Kiss1-MC4RKO female mice (**Figure 1*A, B***).

MC4R in Kiss1 neurons is required for female reproduction.

Because Kiss1-MC4RKO females showed altered puberty onset, we further investigated their reproductive phenotype. Interestingly, Kiss1-MC4RKO female mice displayed normal BW

throughout the time of the study (up to PND150) **(Figure 2*A*)**; however, they presented with irregular estrous cycles with predominantly more time spent in diestrus (P=0.0028) and less time spent in estrus (P=0.0067) than their control littermates (**Figure 2*B, S3a, b***). The assessment of the pulsatile release of LH every 10 min over 180 min revealed no change in the total number of pulses between groups but a significant increase in basal LH release (P=0.04) in Kiss1-MC4RKO female mice (0.42±0.03) compared to controls (0.34±0.02) (**Figure 2*C-H***). The analysis of the gene expression of the "KNDy" systems in the ARH, which control the GnRH pulse generator (15), revealed normal expression levels of *Kiss1*, *Tac2* and *Tacr3*, but significantly lower expression of *Pdyn* (P=0.0067, Kiss1-MC4RKO: 0.78±0.038 vs controls: 1.00±0.019) (**Figure 2*I-L***). The conserved expression of *Kiss1*, *Tac2* and *Tacr3* correlates with the preserved LH pulse frequency and amplitude in Kiss1-MC4RKO mice, while the lower inhibitory tone of dynorphin (**Figure 2*I***) correlates with the higher basal LH levels (**Figure 2*G***). However, the mRNA expression of these genes, alone, does not necessarily reflect changes of their activities. To assess the contribution of MC4R signaling in Kiss1 neurons to the induction of ovulation through the preovulatory LH surge, Kiss1-MC4RKO females and control littermates were submitted to an LH surge induction protocol that showed the induced LH surge was significantly blunted in the Kiss1-MC4RKO females (P=0.0091), while the protocol clearly evoked the expected afternoon rise of LH in control mice (**Figure 2*M***). In line with these findings, the ovaries of Kiss1-MC4RKO females displayed fewer corpora lutea, markers of recent ovulation (P=0.0054, Kiss1-MC4RKO: 0.80±0.37 vs controls: 2.80±0.37), in addition to increased cystic follicles (P=0.0337, Kiss1-MC4RKO: 1.60±0.40 vs controls: 0.40±0.24) (**Figure 2*N-P***), which correlate with decreased fertility as observed by the extended time to deliver pups (*i.e.* longer time to get pregnant) (P=0.0030, Kiss1-MC4RKO: 30.30±4.60 vs controls: 20.88±0.22), and fewer pups per litter (P=0.0095, Kiss1-MC4RKO: 6.66±0.55 vs controls: 8.44±0.24) (**Figure 2*S, T***).

The increase in serum LH levels and decreased ovulation observed in the Kiss1-MC4RKO females is reminiscent of polycystic ovary syndrome (PCOS) mouse models (22, 23). Thus, we investigated whether Kiss1-MC4RKO females display a PCOS-like phenotype. We analyzed circulating levels of testosterone (T) and anti-müllerian hormone (AMH), which are frequently elevated in PCOS models (24). The Kiss1-MC4RKO females expressed normal T and AMH levels compared to control mice in diestrus (**Figure 2*Q, R***). Thus, we can exclude a PCOS-like reproductive phenotype mediated by the lack of melanocortin signaling on Kiss1 neurons.

Re-insertion of MC4R in Kiss1 neurons of MC4RKO mice improves reproductive function. Kiss1-MC4RKO females displayed reproductive abnormalities resembling those described in MC4RKO females (11-13). Thus, we hypothesized that the reproductive defects described for the MC4RKO mice would be, at least in part, due to the absence of MC4R signaling in Kiss1 neurons. To further investigate this hypothesis, we generated mice that do not express *Mc4r* anywhere (MC4R-LoxTB, *i.e.* MC4RKO) or that express *Mc4r* only in Kiss1 neurons (*Kiss1-cre:MC4R-loxTB*). The specific re-insertion of *Mc4r* within Kiss1 neurons in the *Kiss1-cre:MC4R-loxTB* mice was confirmed through RNAscope (**Figure S2*A*).** *Mc4r* expression was not detected in the PVN of these mice (**Figure S2*B***), and it was only detected in Kiss1 neurons in the *Kiss1-cre:MC4R-loxTB* mice. Puberty onset was assessed daily from weaning age through the monitoring of vaginal opening (VO) and first estrus (FE). MC4R-LoxTB and *Kiss1-cre:MC4R-loxTB* female mice displayed normal timing of puberty onset compared to their control littermates, as assessed by VO (P=0.104, MC4R-LoxTB: 30.86±1.90 vs *Kiss1-cre:MC4R-loxTB: 30.09*±1.00 vs controls: 27.57±0.81), and FE (P=0.8472, MC4R-LoxTB: 35.14±2.46 vs *Kiss1-cre:MC4R-loxTB: 34.55*±1.64 vs controls: 35.80±0.84) (**Figure 3*A, B***), despite displaying significantly higher body weight at the time of puberty onset (P=0.0001, MC4R-LoxTB: 15.49±0.50 vs *Kiss1-cre:MC4R-loxTB:* 15.54±0.40 vs Controls: 13.29±0.30) (**Figure 3*C***). As expected, MC4R-LoxTB females (MC4RKO) displayed increased body weight

(**Figure 3D**) and an array of reproductive impairments that included: irregular estrous cycles with significantly more days in diestrus (P=0.0016) and fewer days in estrus (P=0.0317) compared to controls (**Figure 3*E, S3c, e***), significantly higher AUC (MC4R-LoxTB: 109.6±2.39 vs Controls: 80.36±9.05) serum LH levels characterized by higher basal (MC4R-LoxTB: 0.48±0.02 vs Controls: 0.37±0.06) and amplitude levels per LH pulse (MC4R-LoxTB: 0.730±0.009 vs Controls: 0.58±0.07) (**Figure 3*F-J***), and fewer corporal lutea (P=0.0366, MC4R-LoxTB: 0.80±0.80 vs Controls: 4.20±1.15) (**Figure 3*K, L***), recapitulating the same reproductive phenotype observed in Kiss1-MC4RKO mice despite the differences in BW. Re-introduction of MC4R into Kiss1 neurons in *Kiss1-cre:MC4R-loxTB* mice completely recovered estrous cyclicity, which was similar to controls (diestrus: P=0.1932, proestrus: P=0.8262, estrus: P=0.0547, compared to controls) (**Figure 3*E, S3c, d*)** despite *Kiss1-cre:MC4R-loxTB* mice showing the same degree of obesity as MC4R-LoxTB mice (**Figure 3*D***), indicating that obesity *per se* was not mediating the irregular estrous cycles in MC4RKO mice. As indicated above, MC4R-LoxTB mice display higher overall circulating LH levels, and this feature was also recovered by the re-insertion of MC4R in Kiss1 neurons of *Kiss1-cre:MC4R-loxTB* mice (basal LH: 0.32±0.04, LH amplitude: 0.48±0.04, LH pulses/180min: 2.40±0.67 and AUC: 70.62±7.15 compared to controls) (**Figure 3*G-J***), further confirming that the melanocortin action on Kiss1 neurons is required for the normal control of gonadotropin release. Despite these significant improvements in reproductive function, *Kiss1-cre:MC4R-loxTB* mice presented fewer corpora lutea than controls (0.80±0.80), similar to MC4R-LoxTB mice, suggesting that an ovulatory impairment still persists (**Figure 3*K, L***). While tonic LH release and estrous cyclicity are predominantly controlled by $Kiss1^{ARH}$ neurons, ovulation is mediated by the induction of the preovulatory LH surge by $Kiss1^{AVPV/PeN}$ neurons. It is possible that the metabolic signals derived from their obese phenotype, and/or the absence of the direct action of MC4R in GnRH neurons (16, 25) prevents the complete recovery of ovulation in *Kiss1-cre:MC4R-loxTB* mice. Both genetic models displayed significantly lower T (MC4R-LoxTB: 28.50±6.20 vs *Kiss1-cre:MC4R-*

loxTB: 31.22±3.90 vs Controls: 62.84±16.53) and AMH (MC4R-LoxTB: 150.6±22.0 vs *Kiss1-cre:MC4R-loxTB:* 146.9±10.8 vs Controls: 321.8±15.7) levels than control mice in diestrus (**Figure 3*M, N***). Therefore, we can exclude, once again, a PCOS-like reproductive phenotype mediated by the lack of melanocortin signaling.

Kiss1^{ARH} neurons are excited by MC4R agonists.

Based on the expression of *Mc4r* in Kiss1 neurons and the reproductive impairment found after *Mc4r* deletion within Kiss1 neurons (**Figure 2**), we hypothesized that Kiss1^{ARH} neurons are direct targets of melanocortins and would respond to MC4R activation. Initially we did whole-cell, voltage clamp recordings in Kiss1^{ARH} neurons (**Figure 4*A***). *Kiss1-Cre* x Ai32 or *Kiss1-Cre* AAV-injected mice underwent ovariectomy (OVX) and were given estradiol (E2) replacement (*see Methods*). We targeted fluorescent cells for recording which were isolated synaptically by bathing the slices in tetrodotoxin (TTX, 1 μM). Focal application of the high-affinity melanocortin receptor agonist melanotan II (MTII, ~250 nM) elicited a small inward current in half of the isolated Kiss1^{ARH} cells (10/21) (**Figure 4*B*)**. Next, we examined if the E2 state affected MTII response by recording from Kiss1^{ARH} neurons from OVX females and found two thirds (6/9 cells) responded, but there was no significant difference in the average current (**Figure 4*C***). Finally, it must be noted that at this concentration MTII is a non-selective MCR agonist, so we followed up using a perfusion of the MC4R-selective agonist THIQ (100 nM) to determine if activation of MC4Rs alone was sufficient to invoke a postsynaptic response in Kiss1^{ARH} neurons from OVX+E2 females. Similar to MTII, THIQ was able to elicit an excitatory inward current in Kiss1^{ARH} neurons (4/5 cells, -7.4±0.5 pA), indicating MC4R activation is sufficient (**Figure 4*D***).

POMC neurons synapse directly with Kiss1^{ARH} neurons.

Based on the pharmacological activation of MCRs, we wanted to address whether POMC^{ARH} neurons are the source of melanocortins to excite Kiss1^{ARH} neurons directly. To answer this question, we injected an AAV-EF1α-DIO-ChR2:mCherry vector into the ARH of adult *Pomc-Cre* female mice (**Figure 4*E***) (24). After 2-4 weeks we did whole cell recordings from putative Kiss1^{ARH} neurons and looked for a response to high frequency optogenetic stimulation of POMC fibers in OVX + E2-treated females (**Figure 4*F***). We were able to confirm that these were Kiss1 neurons based on the presence of a persistent sodium current and/or *post hoc* identification by scRT-PCR (40/77) cells, **Figure 4*G***). While this current is more prevalent in the AVPV Kiss1 population, Kiss1 neurons are the only ARH neurons to display this electrophysiological "fingerprint" of a pronounced I_{NaP} paired with a high capacitance and a low input resistance (26). Additionally, while recording from putative Kiss1^{ARH} neurons, we optogenetically stimulated POMC fibers at low frequency (1 Hz, 5 ms, 470 nm light) and recorded fast postsynaptic inward currents. The fast kinetics of the EPSC are also a tell-tale sign of an ionotropic glutamatergic response (27). Previously, CNQX was sufficient to block similar excitatory ESPCs in other postsynaptic targets of POMC neurons (28). While the consistent latency from optogenetic stimulus and current response was indicative of a single synaptic delay, we wanted to establish that it was a direct synaptic connection, as we have previously shown for output of POMC neurons (28) and Kiss1 neurons (29-31). First, we abrogated the optogenetic response with the addition of TTX (1 μM) to the bath, and then we were able to rescue the postsynaptic glutamate response with the addition of the K^+ channel blockers 4-aminopyridine (4-AP; 0.5 mM) and tetraethyl ammonium (TEA; 7.5 mM) (**Figure 4*H***). K+ channel block enables the calcium influx from ChR2 activation in the presynaptic terminals to be sufficient to restore vesicle fusion. Therefore, there appears to be no intervening synapses between POMC and the downstream Kiss1^{ARH} neurons.

Previously we found that E2 increases glutamate release from POMC neurons by increasing *Vglut2* (28). Therefore, we compared the postsynaptic glutamatergic responses following two

optogenetic stimuli (50 ms interval between light flashes) in Kiss1^{ARH} neurons from OVX + vehicle versus OVX + E2-treated female mice (**Figure 4*I***). As anticipated, we found that treatment with E2 increased the probability of glutamate release from POMC neurons onto Kiss1^{ARH} neurons based on the significant decrease in the paired pulse ratio of the two stimuli (32) (**Figure 4*J***). Although in the present study we used an *in vivo* treatment paradigm, we know from previous studies that this augmentation of glutamate release can happen quite rapidly after a brief exposure to E2 *in vitro* (within 15 min) (28). Therefore, Kiss1^{ARH} neurons are excited by the glutamatergic input from POMC neurons in an E2-dependent manner.

Next, we tested for a melanocortin response using a high frequency stimulation protocol known to elicit peptide release (33). Only cells displaying a glutamatergic response were tested. Indeed, high frequency stimulation evoked an excitatory inward current (**Figure 4*K***) that was blocked by the selective MC3/4R antagonist SHU 9119 (**Figure 4*L***). However, the number of high frequency responses seen in Kiss1 neurons was unexpectedly infrequent and relatively small (4/16, 25%, mean inward current: -1.4±3.1 pA) compared to the efficacy of pharmacological MCR activation. E2-treatment enhances *Pomc* expression and β-endorphin labeling (34) (35), but the effect, if any, on αMSH release or the MCRs in Kiss1 neurons is unknown. We suspected that the high frequency stimulation was eliciting co-release of αMSH and β-endorphin, which would exert oppositive effects on a postsynaptic cell. In order to isolate melanocortin signaling we pretreated slices with the non-selective opioid antagonist naloxone (1 μM) and found an increase in the likelihood and magnitude of a response to high frequency stimulation (9/23, 40%, mean inward current: -7.6±2.9 pA) (**Figure 4*M***).

Together these optogenetic findings reinforced our pharmacological results showing that Kiss1^{ARH} neurons are excited by MCR agonists. Additional studies would need to be done to identify the cation conductance that is affected by the MC4R signaling cascade in Kiss1^{ARH}

neurons, but clearly we have established that there are excitatory glutamatergic and peptidergic inputs from POMC to Kiss1^{ARH} neurons.

Kiss1$^{AVPV/PeN}$ neurons are inhibited by MC4R agonists.

Having established a direct, excitatory projection from POMC to Kiss1^{ARH} neurons, we next examined POMC inputs to Kiss1^{AVPVPeN} neurons. First, we used immunocytochemistry to label fibers expressing αMSH to demonstrate that POMC fibers densely innervated the AVPV/PeN area (**Figure 5*A***). Next, we recorded from AVPV neurons in slices taken from OVX+E2, POMC-Cre mice injected with AAV1-DIO-YFP:ChR2 into the ARH (**Figure *5B***). We targeted cells along the ventricle in the AVPV and PeN, surrounded by YFP terminals, and Kiss1$^{AVPV/PeN}$ neurons were identified based on the expression of several endogenous conductances (I_{NaP}, T-type calcium current, h-current) that are unique to these neurons (26, 36). We recorded a direct glutamatergic synaptic response following optogenetic stimulation in six neurons, which was further verified through pharmacological "rescue" of the synaptic response in the majority (5/6) neurons tested (**Figure *5C***), indicating that POMC neurons make direct monosynaptic connections with Kiss1$^{AVPV/PeN}$ neurons.

We next hypothesized that Kiss1$^{AVPV/PeN}$ neurons would be excited by exogenous application of melanocortin agonists because the receptor is typically Gs-coupled (37, 38). We did whole-cell, voltage clamp recordings from Kiss1$^{AVPV/PeN}$-Cre::Ai32 neurons, which were isolated synaptically by bathing the neurons in TTX (1 μM), from OVX females. For these experiments, we tested the response to the high affinity melanocortin receptor agonist MTII (500 nM). Surprisingly, we consistently measured an outward (inhibitory) current that could be reversed on washout of MTII (**Figure 5*D***). This outward current was associated with an increase in a K^+ conductance based on the current-voltage plot *(i.e.,* the outward current reversed at ~E_{K+}, **Figure 5E**). Also, the inwardly-rectifying I/V could indicate that MC4R is coupled to activation of inwardly-rectifying K^+ channels as has been previously reported for MC4R signaling in pre-autonomic

parasympathetic neurons in the brainstem (39). We hypothesized that the coupling could be modulated by E2 via a $G\alpha_q$-coupled membrane estrogen receptor (Gq-mER) as we have previously demonstrated in POMC neurons (40-42). For these experiments, we again utilized OVX females and targeted $Kiss1^{AVPV/PeN}$-Cre::Ai32 neurons. Once in the whole-cell voltage-clamp configuration, we perfused the slices with STX (10 nM), a selective ligand for the putative Gq-mER (42), and tested the response to the MTII. Indeed, the outward current (inhibitory) response to MTII was completely abrogated and even reversed by STX (**Figure 5*F, G***). The short-term (bath) treatment with STX ensured that there was no desensitization of the Gq-mER with longer-term (*in vivo*) treatment with E2. Therefore, estrogen receptor activation can rapidly uncouple (*i.e.,* desensitize) the MC4R inhibitory response in $Kiss1^{AVPV/PeN}$ neurons. We would predict that the intracellular signaling cascade for the heterologous desensitization is similar to what we have elucidated in POMC neurons (42), but this will need to be determined in future experiments. We next investigated the response in vehicle-treated, OVX females. Indeed, $Kiss1^{AVPV/PeN}$ neurons were even more inhibited by the same MTII exposure (**Figure 5*G***). Therefore, in contrast to $Kiss1^{ARH}$ neurons, the MC4R appears to be coupled to opening of K^+ channels in $Kiss1^{AVPV/PeN}$ neurons. To further establish whether the MTII was having pre- or postsynaptic effects, we measured the glutamatergic mEPSCs before and after melanocortin receptor activation. We found there was no significant effect on the frequency (**Figure 5H**), but there was an effect on the amplitude (**Figure 5I**). This further supports a postsynaptic locus of STX's effects. However, *posthoc* comparisons found STX increased amplitude compared to both OVX and OVX+E. This result hints at a membrane delimited effect as STX is a much more potent agonist for Gq-mER than E2 (43).

Discussion

Our findings show that melanocortins act directly on Kiss1 neurons to contribute to the metabolic regulation of fertility, in line with previous reports showing that αMSH stimulates LH

release in a kisspeptin-dependent manner (14) and that Kiss1 neurons express the melanocortin receptor MC4R (18-21). Several studies in humans have linked *Mc4r* mutations to reproductive abnormalities, including precocious puberty (9), PCOS (10), and hypogonadism (8). However, a direct association between *MC4R* mutations and reproductive function, independent from the obese condition of these patients, has not been identified (6). In the current study, we show that the reproductive impairments observed in MC4R deficient mice, which replicate many of the conditions described in humans, are largely mediated by the direct action of melanocortins via MC4R on Kiss1 neurons and not to their obese phenotype. This is because the ablation of MC4R from Kiss1 neurons largely replicated the reproductive impairments observed in MC4RKO female mice without inducing obesity, and the selective reinsertion of MC4R into Kiss1 neurons of MC4RKO mice significantly improved their reproductive function without changing their obese phenotype. Strikingly, puberty onset was advanced in Kiss1-MC4RKO females. Our findings revealed a low melanocortin expression in the hypothalamus of WT females during pubertal development, characterized by lower levels of *Agrp, Mc4r* and *Mc3r* expression at the time of puberty onset (~PND30). This developmental decline in the expression of melanocortin receptors is in line with the advanced timing of puberty onset in females when MC4R is congenitally ablated from Kiss1 neurons. A recent study using whole body MC3RKO mice showed a trend to delayed puberty onset (19), suggesting a larger role of melanocortins in the timing of puberty onset. Here, we show that in females the combination of MC3R and MC4R action may be necessary for pubertal development. Interestingly, the MC4R-LoxTB and *Kiss1-cre:MC4R-LoxTB* mice do not show an advancement in puberty onset as we observed in Kiss1-MC4RKO mice; however, these mice are obese at the time of puberty onset already, which may affect the timing of sexual maturation independently of MC4R action in Kiss1 neurons. Of note, the findings presented in this study do not rule out the existence of additional sites of action of MC4R in other neuronal populations to regulate reproduction, *e.g.,* GnRH neurons, which also express MC4R (16, 25). Indeed, the lack of full

recovery of the reproductive function in *Kiss1-cre:MC4R-LoxTB* mice suggests that MC4R in Kiss1 neurons is necessary but not sufficient to achieve full reproductive capabilities.

In addition to early puberty onset, Kiss1-MC4RKO females displayed an impaired preovulatory LH surge driving ovulation and had fewer corpora lutea in their ovaries compared to control littermates, further supporting a role of MC4R in regulating ovulation. While MC4R has been documented in the ovary (11), our data of i) impaired LH surge observed in the Kiss1-MC4RKO females (**Figure 2M**), and ii) direct action of αMSH on Kiss1 ARC and AVPV/PeN neuronal populations through MC4R (**Figures 4, 5**) support a CNS role for MC4R in the regulation of fertility. However, an additional effect of MC4R at the level of the ovary cannot be ruled. One possibility is that the genetic deletion of *Mc4r* from *Kiss1* gene may have affected the ovary. However, to test this hypothesis, the co-expression of *Mc4r* and *Kiss1* in the ovary needs to be investigated. Another possibility is that given the partial fertility of these mice, follicles may have developed at different rates, potentially due to irregular secretion of gonadotropins. As a result, fewer follicles would develop and ovulate. In adulthood, the reproductive phenotype observed in Kiss1-MC4RKO and MC4R-loxTB female mice (increased LH, irregular estrous cycles, oligo-ovulation, increased cystic follicles) correlates with the phenotype observed in PCOS mouse models (22, 23). In fact, an association between *MC4R* mutations and PCOS has been reported (10). However, our mouse models failed to display higher levels of circulating androgens or AMH, two of the hallmarks of PCOS (24), suggesting that melanocortin signaling is unlikely to be a main contributing factor in the development of this syndrome.

Our data revealing early puberty onset, augmented LH pulse and impaired LH surge driving ovulation support a direct role of MC4R on the two primary Kiss1 populations regulating these functions (ARH and AVPV/PeN). We further investigated this and found that MC4R signaling excites $Kiss1^{ARH}$ neurons and inhibits $Kiss1^{AVPV/PeN}$ neurons in an estradiol-dependent manner. In $Kiss1^{ARH}$ neurons, bath applied or optogenetically-evoked release of melanocortin agonists induce a direct excitatory inward current. Our studies using whole cell voltage clamp in female

mice were able to detect a melanocortin-mediated inward current in Kiss1^{ARH} neurons that would increase excitability. Previously, an MCR-activation effect was not detected in cell-attached recordings of diestrus females (14, 44). However, cell-attached recordings do not measure a direct response in isolated Kiss1^{ARH} neurons but rather the summation of multiple synaptic inputs to Kiss1^{ARH} neurons. Most importantly, we did not see a difference in the excitatory response in synaptically isolated Kiss1^{ARH} neurons from E2-treated versus vehicle-treated, ovariectomized females. This emphasizes the importance of doing whole-cell recording from isolated Kiss1 neurons. The modulatory actions of POMC^{ARH} neuronal projections to Kiss1^{ARH} neurons can also occur through a) the excitatory action of glutamate in a process that is facilitated in the presence of estradiol, in line with previous publications (33, 45), and b) the inhibitory action of β-endorphin, suggesting that POMC^{ARH} neurons are able to exert a precise regulatory role of the GnRH pulse generator, *i.e.* Kiss1^{ARH} neurons, in response to metabolic challenges. In the AVPV/PeN, MC4R agonists inhibited Kiss1$^{AVPV/PeN}$ neurons in an estradiol-dependent manner, which utilized a $G\alpha_q$-coupled membrane estrogen receptor (STX receptor) to attenuate the inhibitory tone of MC4R in these neurons. Rapid estrogen signaling may act to ease transitions between states. Membrane delimited E2 actions can quickly attenuate or enhance coupling between receptors and signaling cascades. These effects will precede E2-driven changes in gene expression that produce more stable alterations in signaling. This combination of mechanisms will reduce any lag between rises in serum E2 and physiological effects. Considering the abbreviated mouse reproductive cycle, parallel mechanisms acting on different timescales are particularly important.

Our pharmacology data clearly demonstrates the estradiol-dependent action of MC4R in Kiss1$^{AVPV/PeN}$ neurons, suggesting that similar to Kiss1^{ARH} neurons, this population is regulated by melanocortins. The effect of MC4R agonists on Kiss1 neurons in the presence of TTX, suggests a direct synaptic effect without the need of channelrhodopsin-2(ChR2)-assisted circuit mapping. Nonetheless, to further demonstrate this interaction, we provide evidence of profound

innervation of αMSH fibers and the presence of synaptic contact between POMC and Kiss1$^{AVPV/PeN}$ neurons through the optogenetic stimulation of a glutamatergic response in Kiss1$^{AVPV/PeN}$ neurons after low frequency stimulation of POMC terminals. We intentionally avoided high frequency stimulation of POMC terminals to prevent the co-release of β-endorphins (e.g., **Figure 4M**) and their possible additive effect on the inhibitory action of MC4R. Future studies will be aimed at the characterization of the endogenous opioid pathways in the induction of the LH surge.

To date, two instances of MC4R-mediated inhibition have been described in the central nervous system: MC4R can Gi,o couple to open K+ (Kir6.2) channels in parasympathetic preganglionic neurons in the brainstem (39), and MC4R can directly couple to K+ (Kv7.1) channels in the hypothalamic paraventricular nucleus neurons (46). Interestingly, our findings describe an inhibitory role of MC4R in the reproductive neuroendocrine axis. This steroid state dependent effect is particularly relevant because in the context of reproduction, the two populations of Kiss1 neurons are strikingly different in their response to estradiol, where peptide expression in Kiss1^{ARH} and Kiss1$^{AVPV/PeN}$ neurons are inhibited or stimulated, respectively, in order to mount the negative versus positive feedback of sex steroids (15). This differential regulation allows for the episodic versus surge release of GnRH; however, the cellular mechanisms underlying these opposing roles of Kiss1 neurons to the same stimulus, *i.e.* circulating E2 levels, remain unknown. Although there were no differences in the magnitude of the electrophysiological responses to MTII in Kiss1^{ARH} neurons in vehicle- versus E2-treated, ovariectomized females, we cannot rule out that E2 affects other systems activated by the MC4R signaling cascade as recently reported in MC4R expressing neurons of the ventromedial nucleus of the hypothalamus (VMH) (47). Interestingly, puberty onset was advanced in Kiss1-MC4RKO females. This data suggests that the inhibitory tone of MC4R signaling on Kiss1$^{AVPV/PeN}$ neurons might also be involved in the timing of puberty onset, which in turn suggests a role for this female-specific population of Kiss1 neurons in sexual maturation. Furthermore, our findings suggest that

metabolic cues, through the regulation of the melanocortin output onto Kiss1$^{AVPV/PeN}$ neurons, are essential for the timing and magnitude of the GnRH/LH surge. This study suggests that the melanocortin-kisspeptin pathway is one of the multiple pathways essential for the metabolic regulation of the HPG axis. Future studies are warranted to fully elucidate synaptic input and postsynaptic cascades in the POMC-Kiss1$^{AVPV/PeN}$ circuit.

Altogether, our data reveal a differential regulatory action of MC4R in the neural control of GnRH/LH release, participating in both the surge (E2-treated, ovariectomized female) and the pulse-like (ovariectomized female) modes of LH release through the cellular regulation of Kiss1 neurons, which translate into our findings on the conditional knockout of *Mc4r* from Kiss1 neurons (**Figure 6**). These findings are important because the reproductive abnormalities often attributed to obesity in MC4R deficient patients may not be caused by the excess in body weight but, at least in part, by a deficiency in MC4R signaling directly at the level of Kiss1 neurons that affects predominantly the ability to mount a preovulatory LH surge.

Materials and methods:

<u>In-vivo experimental procedures:</u>

Generation of Kiss1-MC4RKO, Kiss1-cre:MC4R-LoxTB and MC4R-LoxTB Transgenic Mice

Kiss1-MC4RKO mice were generated by crossing *Kiss1-cre* knock-in mice and *MC4R*$^{lox/lox}$ mice. *Kiss1-cre* mice (RRID:MGI:6278139) were obtained from Dr. Richard Palmiter (University of Washington, Seattle, WA) (48) and *Mc4r*$^{lox/lox}$ (RRID:IMSR_JAX:023720) were a gift from Dr. Brad Lowell (Beth Israel Deaconess Hospital, Boston, MA) (4). These mice were crossed to generate Kiss1-MC4RKO mice lacking *Mc4r* expression selectively from Kiss1 neurons (*Kiss1-cre*$^{+/-}$; *MC4R*$^{lox/lox}$) and their control littermates (MC4R$^{lox/lox}$). To generate *Kiss1-cre:MC4R-LoxTB*

and *MC4R-LoxTB* mice, *MC4R-LoxTB* mice were purchased from The Jackson Laboratory (MC4R-LoxTB; catalog no. 006414). These mice present with a loxp-flanked transcriptional blocking (LoxTB) sequence preventing normal endogenous gene transcription and translation from the endogenous locus. Homozygous MC4R-loxTB/loxTB mice are devoid of functional MC4R mRNA (MC4RKO mice), while the presence of Cre recombinase on the Kiss1 promotor in *Kiss1-cre* mice will result in the removal of the transcription blocker and subsequent expression of MC4R in tissue-specific sites (*i.e.* Kiss1 neurons) therefore resulting in the generation of *Kiss1-cre*:MC4R-LoxTB (with *Mc4r* expression restored in Kiss1 neurons), their obese control littermates *MC4R-LoxTB* mice (MC4RKO), and their WT controls ($MC4R^{+/+}$). To rule out early embryonic recombination of the $MC4R^{loxTB/loxTB}$ or $MC4R^{lox/lox}$ alleles, we ran PCR assays on tail DNA designed to detect wild-type allele ($MC4R^{+/+}$), undeleted lox ($MC4R^{lox/lox}$) or loxTB alleles ($MC4R^{loxTB/loxTB}$). Genotyping was confirmed by sending tissue to Transnetyx, Inc., for testing by real-time polymerase chain reaction. Mice were housed in Harvard Medical School Animal Resources facilities where they were fed standard mouse chow (Teklad F6 Rodent Diet 8664) and were given *ad libitum* access to tap water under constant conditions of temperature (22–24˚C) and light (12 hr light [07:00]/dark [19:00] cycle).

RNAscope in situ hybridization

To validate the Kiss1-MC4RKO, *Kiss1-cre*:MC4R-LoxTB and MC4R-LoxTB (MC4RKO) mouse models and investigate the co-expression of *Kiss1* and *Mc4r* mRNA in these mice, dual fluorescence ISH was performed using RNAscope (ACD, Multiplex Fluorescent v.2) according to the manufacturer's protocol using the following probes: *Mc4r* (319181-C2) and *Kiss1* (500141-C1). Brains (n=4/group) from WT OVX (for expression in the ARH) and OVX+E2 (for expression in the AVPV/PeN) mice and OVX Kiss1-MC4RKO, *Kiss1-cre*:MC4R-LoxTB and MC4RKO were removed fresh frozen on dry ice, and then stored at -80˚C until sectioned. Five sets of 20 µm sections in the coronal plane were cut on a cryostat, from the diagonal band of

Broca to the mammillary bodies, thaw mounted onto SuperFrost Plus slides (VWR Scientific) and stored at -80˚C until use. A single set was used for ISH experiment (adjacent sections 100 mm apart). Images were taken at 20x magnification of the sections containing AVPV, PeN, and the three rostro-to-caudal levels of the ARH, and Kiss1 neurons expressing (*Kiss1-cre*:MC4R-LoxTB mice) or lacking (Kiss1-MC4RKO mice) *Mc4r* were identified using ImageJ.

Reproductive maturation of Kiss1-MC4RKO, *Kiss1-cre*:MC4R-LoxTB and MC4R-LoxTB mice

To assess the reproductive phenotype of mice with selective reinsertion of *Mc4r* in Kiss1 neurons (*Kiss1-cre*:MC4R-LoxTB, n=11), selective deletion of *Mc4r* from Kiss1 neurons (Kiss1-MC4RKO, n=24), global deletion of *Mc4r* (MC4R-LoxTB, n=7); and their control $MC4R^{lox/lox}$ littermates (n=14), mice were weaned at post-natal day (PND) 21 and were monitored daily for puberty onset. Females were monitored daily for vaginal opening (VO, indicative of the complete canalization of the vaginal cavity) and for first estrus (first day with cornified cells determined by daily morning vaginal cytology) after the day of VO. Body weight (BW) was measured at the day of puberty onset to determine if changes in puberty onset could be due to differences in BW. Estrous cyclicity was monitored in females by daily vaginal cytology, for a period of 15 days, in 6-month-old mice and their respective control littermates (n=5/group). Cytology samples were obtained every morning (9 am), placed on a glass slide and stained with hematoxylin and eosin for determination of the estrous cycle stage under the microscope.

Fecundity test of Kiss1-MC4RKO females

Adult 6-month-old Kiss1-MC4RKO and control littermate female mice (n=9/group) were placed with adult WT males proven to father litters for 90 days and time to deliver pups and number of pups per litter were monitored.

Characterization of the estradiol-induced luteinizing hormone surge

Kiss1-MC4RKO (n=6) and control MC4R$^{lox/lox}$ littermate (n=5) adult female mice were subjected to bilateral ovariectomy (OVX) via abdominal incision under light isoflurane anesthesia. Immediately after OVX, capsules filled with E2 (1 ug/20g BW) were implanted subcutaneously via a small mid- scapular incision on the back. Five days later, mice were subcutaneously injected in the morning with estradiol benzoate (1 ug/20g BW) to produce elevated proestrus-like E2 levels (induced LH surge) on the following day (49). Blood samples were collected at 8am and 7pm; LH levels were stored at -80˚C until measured via LH ELISA.

Ovarian histology and hormone measurements

Bilateral ovariectomy of 6-month-old Kiss1-MC4RKO (n=4), *Kiss1-cre*:MC4R-LoxTB, MC4R-LoxTB and their control littermates (n=5/group) was performed under light isoflurane anesthesia. Briefly, the ventral skin was shaved and cleaned, and one small abdominal incision was made. Once the ovaries were identified and excised, the muscle incision was sutured, and the skin was closed with surgical clips. Ovaries were stored in Bouin's fixative, sectioned, and stained with hematoxylin and eosin at the Harvard Histopathology Core. Corporal lutea were counted in the middle section of each ovary. Serum samples were also collected for analysis of testosterone and anti-müllerian hormone (AMH) levels in these mice. These hormones levels were measured at the University of Virginia Ligand Assay core with the Mouse & Rat Testosterone ELISA assay (reportable average range 10-1600 ng/dL; sensitivity of 10 ng/dL); AMH ELISA assay (reportable average range 0.2 – 15 ng/mL; sensitivity of 0.2 ng/mL).

LH pulsatile secretion profile in gonad intact Kiss1-MC4RKO, *Kiss1-cre*:MC4R-LoxTB and MC4R-LoxTB female mice

To assess the profile of LH pulses secretion, adult 6 months old gonad intact Kiss1-MC4RKO females (n=6), their control Mc4r$^{lox/lox}$ littermates (n=7); and *Kiss1-cre*:MC4R-LoxTB (n=5/group),

MC4R-LoxTB and their control WT females (n=4/group) were handled daily for 3 weeks to allow acclimation to sampling conditions prior to the experiment. Pulsatile measurements of LH secretion were assessed in diestrus by repeated blood collection through a single incision at the tip of the tail. The tail was cleaned with saline and 4 μL of blood was taken at each time point from the cut tail with a pipette. We collected sequential blood samples every 10 minutes over a 180-minute sampling period. Samples were immediately frozen on dry ice and stored at −80 °C until analyzed with LH ELISA as previously described (50). The functional sensitivity of the ELISA assay was 0.0039 ng/ml with a CV% of 3.3%.

LH pulses analysis

LH pulses in mice were analyzed using a custom-made MATLAB-based algorithm. The MATLAB code includes a loop that determines LH pulses as any LH peak: (i) whose height is 20% greater than the heights of the 2 previous values; (ii) 10% greater than the height of the following value; and (iii) the peak at the second time interval needs to be 20% greater than the single value that comes before it to be considered a pulse, as we previously described (51).

LH pulsatility was assessed by measuring: (1) the total secretory mass, assessed by area under the curve (AUC); (2) the LH pulse amplitude, calculated by averaging the 4 highest LH values in the samples collection period for each animal; (3) the basal LH, calculated by averaging the 4 lowest LH values in the samples collection period for each animal; and (4) the total number of pulses throughout the 180 minutes sampling period.

Immunohistochemistry

Animals and Treatment: Coronal brain blocks (2 mm each) from adult female C57BL/6 mice (n=4) were fixed by immersion in 4% paraformaldehyde for ~ 8 hours, cryoprotected in 30% sucrose solution, frozen in isopentane at –55°C, sectioned coronally on a cryostat at 20 μm, and

thaw-mounted onto Superfrost Plus slides (Fisher Scientific, Pittsburgh, PA). The 20 µm sections were stored at –20°C until used for immunocytochemistry.

Immunocytochemistry: The sections were rinsed in PB (0.1M phosphate buffer, pH 7.4) for at least 30 min. Next, sections were incubated with normal serum corresponding to the host for the secondary antiserum (5 % normal serum with 0.3% Triton-X100 in PBS for 30 min), rinsed in PB and then incubated for ~45 h at 4º C with a rabbit polyclonal antiserum against α-MSH (1:2,500). The specificity of this antiserum has been documented (52). After rinsing, sections were first incubated for 2-3 hours at room temperature with biotinylated donkey anti rabbit gamma globulin (IgG; 1:500) and next with streptavidin-Alexa 488 (1:2500). Both the primary and secondary antibodies were diluted in tris-(hydroxymethyl) aminomethane (0.5 %, Jackson ImmunoResearch, Philadelphia, PA) in PB containing 0.7 % seaweed gelatin (Jackson ImmunoResearch, Philadelphia, PA) and 0.5 % Triton X-100 and 3% bovine serum albumin (BSA; Jackson ImmunoResearch, Philadelphia, PA) adjusted to pH 7.6. Following a final rinse overnight, slides were coverslipped with gelvatol containing the anti-fading agent, 1,4-diazabicyclo(2,2)octane (DABCO; Cold Spring Harbor Protocols, 2006).

Imaging: Photomicrographs of labeling were initially acquired using a Nikon E800 fluorescent microscope (Eclipse E800; Nikon Instruments, Melville, NY) equipped with a fiber illuminator (Intensilight C-HGFI; Nikon Instruments) and a high-definition digital microscope camera head (DS-Fi1; Nikon Instruments) interfaced with a PC-based camera controller (DS-U3; Nikon Instruments).

Real time quantitative PCR

i) To investigate the changes in the expression of the melanocortin genes *Agrp*, *Pomc, Mc3r* and *Mc4r* in the MBH during development in prepubertal and pubertal WT females at ages P10 (n=6), P15 (n=6), P22 (n=6), and P30 (n=5), and ii) evaluate the gene expression profile of *Pdyn*, *Kiss1*, *Tac2*, *Tacr3*, in the ARH of adult intact (in diestrus) female Kiss1-MC4RKO (n=6)

and their control MC4R$^{lox/lox}$ littermates (n=3), the brains were removed and rapidly embedded in Tissue-Tek, frozen in −30°C isopentane solution and stored at −80°C until use. Frozen tissue punches were recovered through MBH with a 1 mm diameter canula (53). These tissue punches encompassed the whole MBH from the WT females (figure 1D) and the ARH from the Kiss1-MC4RKO and their control females (Figure 2I). The tissues were homogenized, and total RNA was isolated using TRIzol reagent (Invitrogen) followed by chloroform/isopropanol extraction. RNA purity and concentration were measured via an absorbance spectrophotometer (260/280 nm > 1.8; NanoDrop 1000, Thermo Fisher Scientific). Total RNA (1 µg) was reverse transcribed to cDNA using random hexamers (High-Capacity cDNA Synthesis Kit, Life Technologies). Quantitative real-time PCR assays were performed using SYBR Green RT-qPCR master mix (Applied Biosystems) and analyzed using ABI Prism 7000 SDS software (Applied Biosystems). The cycling conditions were: 2 minutes incubation at 95°C (hot start), 45 amplification cycles (95°C for 30 seconds, 60°C for 30 seconds, and 45 seconds at 75°C, with fluorescence detection at the end of each cycle), followed by melting curve of the amplified products obtained by ramped increase of the temperature from 55°C to 95°C to confirm the presence of single amplification product per reaction. PCR specificity was verified by melting curve analysis and agarose gel electrophoresis. Each sample was run in duplicate to obtain an average cycle threshold (CT) value and relative expression of each target gene was determined using the comparative Ct method (54). The data were normalized to Hypoxanthine Guanine Phosphoribosyltransferase (*Hprt)* expression levels in each sample. Results were expressed as fold differences in relative gene expression with respect to i) P10 for melanocortin genes expression analysis during development in WT mice, and ii) controls for the KNDy genes expression in female Kiss1-MC4RKO mice. The primers used are listed in Table 1.

Gene	Gene length (pb)	Accession #	Primers	Location (nt)	Sequence

Hprt	352	NM_013556.2	Hprt-F	704-728	CCTGCTGGATTACATTAAAGCGCTG
			Hprt-R	377-401	GTCAAGGGCATATCCAACAACAAAC
Agrp	136	NM_001271806	Agrp-F	466-488	GCCTCAAGAAGACAACTGCAGAC
		.1	Agrp-R	580-601	AAGCAGGACTCGTGCAGCCTTA
Pomc	138	NM_001278584	Pomc-F	187-208	CCATAGATGTGTGGAGCTGGTG
		.1	Pomc-R	303-324	CACCTCCGTTGCCAGGAAACAC
Mc4r	101	NM_016977.4	Mc4r-F	552-570	CCCGGACGGAGGATGCTAT
			Mc4r-R	632-652	TCGCCACGATCACTAGAATGT
Pdyn	200	NM_018863.4	Pdyn-F	45-64	ACAGGGGGAGACTCTCATCT
			Pdyn-R	223-244	GGGGATGAATGACCTGCTTACT
Kiss1	129	AF472576.1	Kiss1-F	147-166	GCTGCTGCTTCTCCTCTGTG
			Kiss1-R	256-275	TCTGCATACCGCGATTCCTT
Tac2	234	NM_001199971	Tac2- F	238-257	GCTCCACAGCTTTGTCCTTC
		.1	Tac2- R	452-471	GCTAGCCTTGCTCAGCACTT
Tacr3	159	NM_021382.6	Tacr3-F	759-779	GCCATTGCAGTGGACAGGTAT
			Tacr3-R	898-917	ACGGCCTGGCATGACTTTTA

Data analysis

Statistical data are expressed as means ± SEM, where n represents the number of animals in each study group. The significance of differences between groups was evaluated using unpaired two-tailed Student's t test, or a one- or two-way ANOVA test (with *post hoc* comparisons). Significance level was set at $p<0.05$. All analyses were performed with GraphPad Prism Software, Inc (San Diego, CA).

<u>In-vitro experimental procedures:</u>

Animals:

All animal procedures described in the electrophysiology studies were performed in accordance with institutional guidelines based on National Institutes of Health standards and approved by the Institutional Animal Care and Use Committees at Oregon Health and Science University and Appalachian State University. *Kiss1-cre* (v2) mice (48) were crossed with Ai32 (55) or C57B6J mice. *Pomc-Cre* mice (RRID:IMSR_JAX:005965) (56) were crossed with wildtype C57B6J (RRID:IMSR_JAX:000664) mice. The Ai32 cross was not used with *Pomc-Cre* mice because the gene is transiently expressed during development in some cells fated to be Kiss1 or AgRP cells (57) and early recombinant events lead to persistent expression of the ChR2-mCh fusion protein in non-POMC cells. However, we have previously shown that AAV-driven expression in adult *Pomc-cre* animals is restricted to β-endorphin labeled cells in the ARH (45), avoiding this non-specificity issue. All colonies were maintained onsite under controlled temperature (21-23 ºC) and photoperiod (12:12-h light-dark cycle 0600 to 1800) while receiving ad libitum food (5L0D; LabDiet, St. Louis, MO) and water access. Following surgeries, mice received a *s.c.* dose of 4-5 mg/kg carprofen (Rimadyl; Pfizer Animal Health, New York, NY) and given at least 1 week of recovery.

Ovariectomies:

Seven to ten days prior to each experiment, ovaries were removed as described previously while under isoflurane anesthesia (45). Two days before experiments females received either an injection of sesame oil (50 µl, *sc*; Sigma-Aldrich, St. Louis, MO) or a priming dose (0.25 µg /50 µl sesame oil, *sc*) of E2 benzoate (Sigma-Aldrich, St. Louis, MO) in the morning. On the following day, oil or a high (1.5 µg) dose of E2 benzoate, which generates an induced LH surge, was administered (58). Circulating levels of E2 were verified by the uterine weights (<25 mg for OVX and >95 mg for OVX E2-treated) at the time of euthanasia (58).

AAV Delivery:

Bilateral ARH injections of AAV1-Ef1a-DIO-ChR2:mCherry (RRID:Addgene_20297) or AAV1-Ef1a-DIO-ChR2:YFP (RRID:Addgene_20298) were performed on adult *Kiss1-cre* mice or *Pomc-cre* mice on a stereotaxic frame under isoflurane anesthesia. ARH injection coordinates were anteroposterior (AP): −1.10 mm, mediolateral (ML): ± 0.30 mm, dorsoventral (DL): −5.80 mm (surface of brain z = 0.0 mm); 400 nl of the AAV (2.0 x 10^{12} particles/ml) was injected (100 nl/min) into each position. Mice were given carprofen for analgesia and allowed to recover for at least two weeks before euthanasia.

Visualized whole-cell patch recordings:

Hypothalamic coronal brain slices (240 um) were made from female mice, using a Leica VT1000S vibratome, in ice cold cutting solution bubbled with O_2/$C0_2$ (95%/5%). Slices were then transferred to a holding chamber with artificial cerebrospinal fluid bubbled with the same gas mix and allowed to recover for at least 1 hour. For recordings, slices were placed in a perfusion chamber and visualized with an Olympus BX51W1 using either differential infrared contrast or oblique illumination. Kiss1 neurons in the ARH or AVPV/PeN were targeted for electrophysiological recordings as done previously and described below (59, 60). Final concentration was calculated based on the drug in the known volume of the bath. Perfused drugs (TTX, naloxone, and STX) were constantly circulated and given at least 10 minutes to reach maximal effect. Focal application of drugs (MTII and THIQ) was done with the pump stopped (10-20 minutes). 0.3 to 1 µl was directly added to the known volume of the bath to achieve the desired final concentration. This approach enables precise timing of recordings and reduces the risk of receptor desensitization.

Solutions/drugs:

Standard vibratome slicing, external, and internal recording solutions were utilized as previously described (59, 60). Tetrodotoxin was purchased from Alomone Labs (Jerusalem, Israel),

Melanotan II and αMSH from Tocris (Minneapolis, MN). TEA, 4-AP, 17β-estradiol benzoate, and Naloxone were purchased from Millipore-Sigma. STX was produced by AAPharmaSyn, LLC (Ann Arbor, MI) under contract.

Electrophysiology data analysis:

Electrophysiological data were analyzed using Clampfit 10/11 (Molecular Devices) and Prism 7/10 (Dotmatics). All values are expressed as Mean ± SEM. Comparisons between two groups were made using un-paired Student's t-test or between multiple groups using an ANOVA (with *post hoc* comparisons) with p-values < 0.05 considered significant. When variances differed significantly, Mann-Whitney U test was used instead.

Targeting of Kiss1 neurons for electrophysiological recordings.

For non-optogenetic experiments, brain slices were taken from AAV injected Kiss1-Cre AAV or Kiss1xAi32 female mice. Ai32 mice (RRID:IMSR_JAX:024109, C57BL/6 background) carry the floxed ChR2 (H134R)-EYFP gene in their Gt(ROSA)26Sor Locus (55), allowing its expression in a Cre-dependent manner. Due to concerns of nonspecific expression (61), we previously validated this model using single cell RT-PCR and documented that *Kiss1* mRNA was detectable in 99% of individually harvested eYFP cells (n=126). In addition, we have used both AAV injected Kiss1-Cre AAV or Kiss1xAi32 female mice and found no differences in electrophysiological results (59). We used AAV injected POMC-Cre female mice and avoided small soma, high input resistance (>800 MΩ), ventrally located cells that are typically NPY/AgRP neurons. Instead, we targeted larger, more dorsomedial neurons in the ARH while avoiding fluorescent (POMC) cells. Unlike ARH Kiss1 neurons, POMC neurons do not make reciprocal projections, so uninfected POMC neurons do not display monosynaptic EPSCs in

response to optogenetic stimulation. Next, we used a ramp IV protocol to probe for the presence of a persistent sodium current (I_{NaP}). While this current is more prevalent in the AVPV Kiss1 population, Kiss1 neurons are the only ARH neurons to display this electrophysiological "fingerprint" of a pronounced I_{NaP} paired with a high capacitance and low input resistance (26). Finally, we also harvested the cytosol at the end of all recordings and measured the expression of Kiss1. Only cells that expressed a persistent sodium current and/or expressed *Kiss1* mRNA were included in final analysis (n = 40 ARH & 6 AVPV).

Acknowledgments:

The authors would like to recognize the excellent technical expertise of Ms. Martha A. Bosch (tissue preparation, immunohistochemical procedure and single cell RT-PCR of recorded neurons). In addition, we thank Dr. Rona Carroll for her assistance at Harvard Medical School and Mr. Cole Martinson, a student worker in the Ronnekleiv/ Kelly laboratories, for his assistance with genotyping and care of mouse colonies at OHSU. The University of Virginia Center for Research in Reproduction Ligand Assay and Analysis Core is supported by the Eunice Kennedy Shriver NICHD/NIH (NCTRI) Grant P50-HD28934. This work was supported by PHS MPI grant DK68098 to MJK and OKR; HD090151, HD099084 and DK133760 to VMN, and The Charles A. King Trust Postdoctoral Research Fellowship Award, The Lalor Foundation Postdoctoral Fellowship Award, the Women's brain initiative Fellowship Award, the ROSA SCORE pilot grant (supported by NIH Research Grant U54 AG062322 funded by The National Institute on Aging (NIA) and Office of Research on Women's Health (ORWH)) and the IBRO-ISN Research Fellowship Award to RT, and startup funds from Appalachian State University to TLS.

Authors contribution:

RT, TLS, MJK and VMN conceived and designed the study; RT, TLS, KF, CJH, EM, AG, KW, SL, EAM, OKR performed the experiments. RT, TLS, OKR, MJK and VMN analyzed data. RT, TLS and VMN wrote the manuscript with input from all the authors.

Declaration of interests:

The authors declare they have no competing interest.

Figure legends:

Figure 1. *Mc4r* expressed in Kiss1 neurons determines the timing of puberty onset. Kiss1-MC4RKO females display advanced puberty onset, assessed by daily monitoring of vaginal opening **(A)** and first estrus **(B)**, as documented by cumulative percent and mean age of animals at vaginal opening **(A)** and first estrus **(B)** in Kiss1-MC4RKO females (n=24) compared to WT littermates (n=19). *p<0.05 by Student's t-test. Data presented as the mean± SEM. **(C)** Female Kiss1-MC4RKO (n=19) have normal body weight at the time of puberty onset compared to their WT littermates (n=15). **(D)** Ontogeny expression of melanocortin genes (*Agrp*, *Pomc*, *Mc4r and Mc3r*) in the ARH of WT female mice at different postnatal pre-pubertal and pubertal ages: P10, P15, P22 and P30, normalized to the housekeeping gene *Hprt*. (*n values*: females at P10 (n=6), P15 (n=6), P22 (n=6), and P30 (n=5)). Groups with different letters are significantly different (p<0.05), as determined by one-way ANOVA followed by the Student-Newman-Keuls test. Data presented as the mean± SEM.

Figure 2. Deletion of MC4R from Kiss1 neurons impairs fertility in Kiss1-MC4RKO females.

(A) Female Kiss1-MC4RKO (n=19) have normal body weight from weaning and until post-natal day (PND) 150 compared to their WT littermates (n=15). **(B)** Kiss1-MC4RKO females displayed irregular estrous cycles with a longer time in diestrus and a shorter time in estrus compared to control females. ** P < 0.01 Two-way ANOVA. **(C, D)** Pattern of LH pulsatility was analyzed in gonad intact Kiss1-MC4RKO (n=6) and control (n=7) females. # Represents LH pulses. **(E)** LH total secretory mass assessed by area under the curve (AUC), **(F)** LH pulse amplitude, **(G)** Basal LH and **(H)** Total number of pulses /180 min were analyzed. *p<0.05 by Student's t-test. The expression of the KNDy genes *Pdyn* **(I)**, *Kiss1* **(J)**, *Tac2* **(K)** and *Tacr3* **(L)**, was assessed in the ARH of adult Kiss1-MC4RKO (n=6) and control (n=3) females. **p<0.01 by Student's t-test. Data presented as the mean± SEM. **(M)** Kiss1-MC4RKO (n=6) and control (n=5) females were subjected to an LH surge induction protocol. LH samples were collected in the morning (AM [8 a.m.]) and evening (PM [7 p.m.]) after lights off. **P < 0.01, Two-way ANOVA followed by Bonferroni *post hoc* test. **(N)** Ovarian histology shows a decrease in the number of corpora lutea (CL, **O**) and increase in the number of cystic follicles (CF, **P**) of Kiss1-MC4RKO compared to controls (n=5/group). # represents cystic follicles. Serum levels of Testosterone **(Q)** and AMH **(R)** in adult gonad intact Kiss1-MC4RKO and control females (n=5/group). Student t test for unpaired samples. Data presented as the mean± SEM. Kiss1-MC4RKO females display impaired fertility characterized by increased time to deliver pups **(S)** and decreased number of pups per litter **(T)**, (n=9/group). *p<0.05 and **p<0.01 by Student's t-test. Data presented as the mean± SEM.

Figure 3. Re-insertion of MC4R in Kiss1 neurons restores estrous cyclicity and LH pulsatility in Kiss1-cre:MC4R-LoxTB females.

(A, B) *Kiss1-cre*:MC4R-LoxTB (n=11) and MC4R-loxTB (MC4RKO) (n=7) displayed normal puberty onset as compared to their control littermates (n=14), as documented by cumulative

percent and mean age of animals at vaginal opening and first estrus. **(C)** *Kiss1-cre*:MC4R-LoxTB and MC4R-loxTB both had significantly higher body weights at the time of puberty onset compared to their controls. **P < 0.01, *** P < 0.001 by one way ANOVA. **(D)** MC4R-loxTB (n=7) and *Kiss1-cre*:MC4R-LoxTB (n=11) females displayed significantly higher body weight than their littermates (n=10) from post-natal day 30 onwards, *p<0.05 and **P < 0.01. Data presented as the mean± (SEM). **(E)** MC4R-loxTB females displayed irregular estrous cycles, presenting longer time in diestrus and shorter time in estrus compared to control females, while *Kiss1-cre*:MC4R-LoxTB females displayed regular estrous cyclicity, similar to controls. *p<0.05, **P < 0.01, *** P < 0.001, ****P < 0.0001, Two-way ANOVA. Data presented as the mean± SEM. **(F)** Pattern of LH pulsatility analyzed in gonad intact MC4R-loxTB (n=4), *Kiss1-cre*:MC4R-LoxTB (n=5) and control littermates females (n=5). LH samples were collected every 10 min for 180 minutes; # represents LH pulses. **(G)** LH total secretory mass, **(H)** LH pulse amplitude, **(I)** basal LH, and **(J)** total number of pulses /180 min were assessed. *p<0.05, **P < 0.01 by one way ANOVA. **(K)** Representative samples of ovarian histology from MC4R-loxTB, *Kiss1-cre*:MC4R-LoxTB and control females (n=5/group); CL: Corpora lutea. Data are presented as the mean± SEM. **(L)** Ovarian histology showed a significant decrease in the number of corpora lutea in the MC4RKO and *Kiss1-cre*:MC4R-LoxTB compared to controls. Groups with different letters are significantly different. Serum levels of **(M)** Testosterone and **(N)** AMH in adult gonad intact females MC4R-loxTB, *Kiss1-cre*:MC4R-LoxTB and their control littermates. *p<0.05, ****P < 0.0001, One Way ANOVA. Data are presented as the mean± SEM.

Figure 4. Kiss1^{ARH} neurons are activated by melanocortin agonists and respond to optogenetic stimulation of POMC neurons.

(A) Slices were taken from *Kiss1-cre* injected (confocal image) brains to target fluorescent cells (arrowhead) for recording (white outline over electrode). **(B)** Whole cell voltage clamp recording of Kiss1^{ARH} neurons following the direct application of the high affinity melanocortin receptor

agonist melanotan II (MTII, 250 nM) was added directly to the bath and the response was compared between slices from OVX and OVX+E females. **(C)** While the average inward current was slightly higher in the OVX+E state, this was not a significant difference (Student's t-test for unpaired samples, $p>0.05$). **(D)** The MC4R-selective agonist THIQ (100 nM) was perfused, and excitatory inward currents were generated in $Kiss1^{ARH}$ neurons. **(E)** Images are of AAV-driven labeling of POMC cells as seen through the confocal. **(F)** Using the AAV-driven expression of channelrhodopsin in adult *Pomc-cre* mice, high frequency stimulation elicited a slow inward current in Kiss1 neurons. **(G)** The identity of cells was confirmed through the presence of a persistent sodium current (see (26)) and/or with RT-PCR of harvested cytoplasm showing *Kiss1* expression. (Gel: MM=molecular marker, TC=tissue controls). **(H)** A direct synaptic projection from POMC to $Kiss1^{ARH}$ neuron (*posthoc* identified) was confirmed using the "rescue" protocol: 1, baseline glutamatergic responses were initially generated (black trace); 2, then action potentials were eliminated by blocking voltage-gated sodium channels with TTX and the postsynaptic response (red trace); 3, blockade of potassium channels facilitated calcium entry into the terminal through ChR2 to release synaptic vesicles, "rescuing" the postsynaptic glutamate response (green trace). **I)** Glutamatergic responses were also often observed, particularly in the ventral ARH. As seen when targeting low input resistance neurons (i.e., $Kiss1^{ARH}$) with low frequency optogenetic stimulation (5 ms pulse, 50 ms inter-spike interval), the first response in OVX + vehicle females was larger relative to the second response in OVX + E2- treated female mice. Representative traces are the average of 30 sweeps. **(J)** The averaged paired-pulse ratio was lower in recordings from estradiol-treated female mice, indicating an increased release probability (Students t-test $p<0.05$,). **(K)** High frequency optogenetic stimulation elicited a small inward current. **(L)** In a different cell, a high frequency inward current was noted before constant perfusion of SHU9119 for 15 minutes (break between traces). When the stimulation protocol was repeated, no inward current was elicited. **(M)** The majority of high frequency responses were inward and only twice was an inhibitory outward

current recorded in identified Kiss1^{ARH} neurons. Perfusion of the non-selective opioid receptor antagonist naloxone reversed the current, eliminating MCR-activation as the mechanism.

Figure 5. Kiss1$^{AVPV/PeN}$ neurons are inhibited by MC4R agonists in an E2-dependent manner.

(A) Immunohistochemistry showing robust labeling of α-MSH fibers in the AVPV/PeN region in OVX+E2 WT female mice. **(B)** Low and high power bright-field images taken during electrophysiology recording in OVX+E2 POMC-Cre mice expressing YFP:ChR2 in the ARH following AAV injection. (left) Low power image shows the location of recorded cells. (right) Higher power image of area from white box inset displaying POMC fibers innervating the area. **(C)** Fibers surrounded putative Kiss1-AVPV neurons (expressing I_{NaP}, IT and I_h) and optogenetic stimuli was able to elicit postsynaptic currents that were eliminated with tetrodotoxin (1 μM), but "rescued" with addition of K^+ channel blockers (4-AP and TEA) which indicates a monosynaptic connection between POMC^{ARH} and Kiss1^{AVPV} neurons. **(D)** Whole-cell voltage clamp recordings were made in ChR2-YFP positive cells in brain slices taken from *Kiss1-cre*:Ai32 female mice. Bath application of melanotan II (MTII, 500 nM) generated an inhibitory outward current in a Kiss1$^{AVPV/PeN}$ neuron from OVX female. As the cell was synaptically isolated using bath-applied tetrodotoxin (TTX, 1 μM) this represents a direct effect. Washout of MTII while still in TTX quickly led to a return to baseline RMP. **(E)** An IV relationship was plotted using voltage steps before and after MTII administration. The crossing at -80 mV (~EK^+) indicates that the opening of K+ channels underlie the MC4R inhibition of Kiss1^{AVPV} neurons. **(F)** In a subset of recordings from OVX brains slices, the selective membrane estrogen receptor (Gq-mER) agonist STX (10 nM) was added to the bath for ~10 minutes prior to addition of MTII. STX pretreatment resulted in either a greatly attenuated outward current or even an inward current as shown in this example. **(G)** The mean outward current was significantly higher when recording in Kiss1$^{AVPV/Pen}$ neurons from brain slices from vehicle-treated, OVX females compared to E2-treated, OVX

females or acute STX-treated brain slices from OVX females (One-way ANOVA $F_{(2,19)}$=12.32, $p<0.001$; Holm-Sidak *posthoc* comparisons found significant differences between all groups; * $p<0.05$, *** $p<0.001$). **(H)** There was no difference in the frequency of mEPSCs after MTII, calculated as a percent of baseline between groups. **(I)** However, there was a significant difference in the mEPSC amplitude (calculated as a percent of baseline) between all groups: main effect $F_{(2,19)}$ =10.58, $p<0.001$. *Posthoc* comparisons using Holm-Sidak found OVX+STX to be different from both OVX ($p<0.001$) and OVX+E ($p<0.05$).

Figure 6. Working model of the neuronal input from POMC ARH to Kiss1 ARH and AVPV populations.

$POMC^{ARH}$ neurons excite $Kiss1^{ARH}$ neurons via glutamate and αMSH release, which activate glutamatergic ionotropic receptors and MC4R, respectively. In low E2 state, αMSH fibers project to the AVPV/PeN, and MC4R inhibit $Kiss1^{AVPV/PeN}$ neurons via opening a K^+ channel. However, in high E2 state, E2 enhances the glutamatergic excitation of both POMC and Kiss1 ARH neurons. E2-treatment rapidly abrogates (uncouples) the inhibitory MC4R signaling in $Kiss1^{AVPV/PeN}$ neurons, allowing greater excitatory actions of $Kiss1^{ARH}$ neurons via enhanced glutamate release (26).

References:

1. Health U. Infertility. 2020 [Available from: http://obgyn.ucla.edu/infertility
2. Andermann ML, Lowell BB. Toward a Wiring Diagram Understanding of Appetite Control. Neuron. 2017;95(4):757-78.
3. Cone RD. Studies on the physiological functions of the melanocortin system. Endocr Rev. 2006;27(7):736-49.
4. Shah BP, Vong L, Olson DP, Koda S, Krashes MJ, Ye C, et al. MC4R-expressing glutamatergic neurons in the paraventricular hypothalamus regulate feeding and are synaptically connected to the parabrachial nucleus. Proceedings of the National Academy of Sciences of the United States of America. 2014;111(36):13193-8.

907 5. Wang K, Mao W, Zhang X, Zhao Y, Fan K, Pan D, et al. Neuroanatomy of melanocortin-4
908 receptor pathway in the mouse brain. Open Life Sci. 2020;15(1):580-7.
909 6. Farooqi IS, Keogh JM, Yeo GS, Lank EJ, Cheetham T, O'Rahilly S. Clinical spectrum of
910 obesity and mutations in the melanocortin 4 receptor gene. The New England journal of
911 medicine. 2003;348(12):1085-95.
912 7. Balthasar N, Dalgaard LT, Lee CE, Yu J, Funahashi H, Williams T, et al. Divergence of
913 melanocortin pathways in the control of food intake and energy expenditure. Cell.
914 2005;123(3):493-505.
915 8. Hainerová IA, Zamrazilová H, Sedláčková D, Hainer V. Hypogonadotropic hypogonadism
916 in a homozygous MC4R mutation carrier and the effect of sibutramine treatment on body
917 weight and obesity-related health risks. Obes Facts. 2011;4(4):324-8.
918 9. Doulla M, McIntyre AD, Hegele RA, Gallego PH. A novel MC4R mutation associated with
919 childhood-onset obesity: A case report. Paediatr Child Health. 2014;19(10):515-8.
920 10. Batarfi AA, Filimban N, Bajouh OS, Dallol A, Chaudhary AG, Bakhashab S. MC4R variants
921 rs12970134 and rs17782313 are associated with obese polycystic ovary syndrome patients in
922 the Western region of Saudi Arabia. BMC Med Genet. 2019;20(1):144.
923 11. Chen X, Huang L, Tan HY, Li H, Wan Y, Cowley M, et al. Deficient melanocortin-4
924 receptor causes abnormal reproductive neuroendocrine profile in female mice. Reproduction
925 (Cambridge, England). 2017;153(3):267-76.
926 12. Sandrock M, Schulz A, Merkwitz C, Schoneberg T, Spanel-Borowski K, Ricken A.
927 Reduction in corpora lutea number in obese melanocortin-4-receptor-deficient mice. Reprod
928 Biol Endocrinol. 2009;7:24.
929 13. Cui L, Tan C, Huang L, Wang W, Huang Z, Geng F, et al. Dapagliflozin partially restores
930 reproductive function in MC4R KO obese female mice. The Journal of endocrinology.
931 2022;254(2):65-76.
932 14. Manfredi-Lozano M, Roa J, Ruiz-Pino F, Piet R, Garcia-Galiano D, Pineda R, et al. Defining
933 a novel leptin-melanocortin-kisspeptin pathway involved in the metabolic control of puberty.
934 Mol Metab. 2016;5(10):844-57.
935 15. Goodman RL, Herbison AE, Lehman MN, Navarro VM. Neuroendocrine control of
936 gonadotropin-releasing hormone: Pulsatile and surge modes of secretion. Journal of
937 neuroendocrinology. 2022;34(5):e13094.
938 16. Israel DD, Sheffer-Babila S, de Luca C, Jo YH, Liu SM, Xia Q, et al. Effects of leptin and
939 melanocortin signaling interactions on pubertal development and reproduction. Endocrinology.
940 2012;153(5):2408-19.
941 17. Manfredi-Lozano M, Roa J, Tena-Sempere M. Connecting metabolism and gonadal
942 function: Novel central neuropeptide pathways involved in the metabolic control of puberty
943 and fertility. Front Neuroendocrinol. 2018;48:37-49.
944 18. Cravo RM, Margatho LO, Osborne-Lawrence S, Donato J, Jr., Atkin S, Bookout AL, et al.
945 Characterization of Kiss1 neurons using transgenic mouse models. Neuroscience. 2011;173:37-
946 56.
947 19. Lam BYH, Williamson A, Finer S, Day FR, Tadross JA, Gonçalves Soares A, et al. MC3R
948 links nutritional state to childhood growth and the timing of puberty. Nature.
949 2021;599(7885):436-41.

950 20. Villa PA, Ruggiero-Ruff RE, Jamieson BB, Campbell RE, Coss D. Obesity alters POMC and
951 kisspeptin neuron crosstalk leading to reduced luteinizing hormone in male mice. The Journal of
952 Neuroscience. 2024:e0222242024.
953 21. Stephens SBZ, Kauffman AS. Estrogen Regulation of the Molecular Phenotype and Active
954 Translatome of AVPV Kisspeptin Neurons. Endocrinology. 2021;162(9).
955 22. Moore AM, Prescott M, Campbell RE. Estradiol negative and positive feedback in a
956 prenatal androgen-induced mouse model of polycystic ovarian syndrome. Endocrinology.
957 2013;154(2):796-806.
958 23. McCarthy EA, Dischino D, Maguire C, Leon S, Talbi R, Cheung E, et al. Inhibiting Kiss1
959 Neurons With Kappa Opioid Receptor Agonists to Treat Polycystic Ovary Syndrome and
960 Vasomotor Symptoms. J Clin Endocrinol Metab. 2022;107(1):e328-e47.
961 24. Dewailly D, Barbotin AL, Dumont A, Catteau-Jonard S, Robin G. Role of Anti-Müllerian
962 Hormone in the Pathogenesis of Polycystic Ovary Syndrome. Frontiers in endocrinology.
963 2020;11:641.
964 25. Roa J, Herbison AE. Direct regulation of GnRH neuron excitability by arcuate nucleus
965 POMC and NPY neuron neuropeptides in female mice. Endocrinology. 2012;153(11):5587-99.
966 26. Zhang C, Bosch MA, Qiu J, Ronnekleiv OK, Kelly MJ. 17beta-Estradiol increases persistent
967 Na(+) current and excitability of AVPV/PeN Kiss1 neurons in female mice. Mol Endocrinol.
968 2015;29(4):518-27.
969 27. Clements JD, Westbrook GL. Activation kinetics reveal the number of glutamate and
970 glycine binding sites on the N-methyl-D-aspartate receptor. Neuron. 1991;7(4):605-13.
971 28. Stincic TL, Grachev P, Bosch MA, Rønnekleiv OK, Kelly MJ. Estradiol drives the
972 anorexigenic activity of proopiomelanocortin neurons in female mice. eNeuro.
973 2018;5(4):e0103-18.2018.
974 29. Qiu J, Nestor CC, Zhang C, Padilla SL, Palmiter RD, Kelly MJ, et al. High-frequency
975 stimulation-induced peptide release synchronizes arcuate kisspeptin neurons and excited GnRH
976 neurons. eLife. 2016;5:e16246.
977 30. Qiu J, Rivera HM, Bosch MA, Padilla SL, Stincic TL, Palmiter RD, et al. Estrogenic-
978 dependent glutamatergic neurotransmission from kisspeptin neurons governs feeding circuits
979 in females. eLife. 2018;7:e35656.
980 31. Stincic TL, Qiu J, Connors AM, Kelly MJ, Rønnekleiv OK. Arcuate and Preoptic Kisspeptin
981 neurons exhibit differential projections to hypothalamic nuclei and exert opposite postsynaptic
982 effects on hypothalamic paraventricular and dorsomedial nuclei in the female mouse. eneuro.
983 2021:ENEURO.0093-21.2021.
984 32. Herman MA, Ackermann F, Trimbuch T, Rosenmund C. Vesicular glutamate transporter
985 expression level affects synaptic vesicle release probability at hippocampal synapses in culture.
986 The Journal of Neuroscience. 2014;34(35):11781-91.
987 33. Qiu J, Rivera HM, Bosch MA, Padilla SL, Stincic TL, Palmiter RD, et al. Estrogenic-
988 dependent glutamatergic neurotransmission from kisspeptin neurons governs feeding circuits
989 in females. Elife. 2018;7.
990 34. Thornton JE, Loose MD, Kelly MJ, Rønnekleiv OK. Effects of estrogen on the number of
991 neurons expressing β-endorphin in the medial basal hypothalamus of the female guinea pig.
992 The Journal of comparative neurology. 1994;341:68-77.

993 35. Petersen SL, Keller ML, Carder SA, McCrone S. Differential Effects of Estrogen and
994 Progesterone on Levels of POMC mRNA Levels in the Arcuate Nucleus: Relationship to the
995 Timing of LH Surge Release. Journal of Neuroendocrinology. 1993;5(6):643-8.
996 36. Zhang C, Tonsfeldt KJ, Qiu J, Bosch MA, Kobayashi K, Steiner RA, et al. Molecular
997 mechanisms that drive estradiol-dependent burst firing of Kiss1 neurons in the rostral
998 periventricular preoptic area. American journal of physiology Endocrinology and metabolism.
999 2013;305(11):E1384-97.
1000 37. Mountjoy KG, Mortrud MT, Low MJ, Simerly RB, Cone RD. Localization of the
1001 melanocortin-4 receptor (MC4-R) in neuroendocrine and autonomic control circuits in the
1002 brain. Molecular Endocrinology. 1994;8(10):1298-308.
1003 38. Yu J, Gimenez LE, Hernandez CC, Wu Y, Wein AH, Han GW, et al. Determination of the
1004 melanocortin-4 receptor structure identifies Ca^{2+} as a cofactor for ligand binding. Science.
1005 2020;368(6489):428-33.
1006 39. Sohn JW, Harris LE, Berglund ED, Liu T, Vong L, Lowell BB, et al. Melanocortin 4
1007 receptors reciprocally regulate sympathetic and parasympathetic preganglionic neurons. Cell.
1008 2013;152(3):612-9.
1009 40. Kelly MJ, Loose MD, Ronnekleiv OK. Estrogen suppresses mu-opioid- and GABAB-
1010 mediated hyperpolarization of hypothalamic arcuate neurons. The Journal of neuroscience : the
1011 official journal of the Society for Neuroscience. 1992;12(7):2745-50.
1012 41. Lagrange AH, Ronnekleiv OK, Kelly MJ. The potency of mu-opioid hyperpolarization of
1013 hypothalamic arcuate neurons is rapidly attenuated by 17 beta-estradiol. The Journal of
1014 neuroscience : the official journal of the Society for Neuroscience. 1994;14(10):6196-204.
1015 42. Qiu J, Bosch MA, Tobias SC, Grandy DK, Scanlan TS, Ronnekleiv OK, et al. Rapid signaling
1016 of estrogen in hypothalamic neurons involves a novel G-protein-coupled estrogen receptor that
1017 activates protein kinase C. The Journal of neuroscience : the official journal of the Society for
1018 Neuroscience. 2003;23(29):9529-40.
1019 43. Qiu J, Bosch MA, Tobias SC, Krust A, Graham SM, Murphy SJ, et al. A G-protein-coupled
1020 estrogen receptor is involved in hypothalamic control of energy homeostasis. The Journal of
1021 neuroscience : the official journal of the Society for Neuroscience. 2006;26(21):5649-55.
1022 44. Sabine Hessler XL, Allan E. Herbison. Direct inhibition of arcuate kisspeptin neurones by
1023 neuropeptide Y in the male and female mouse. Journal of Neuroendocrinology. 2020.
1024 45. Stincic TL, Grachev P, Bosch MA, Ronnekleiv OK, Kelly MJ. Estradiol Drives the
1025 Anorexigenic Activity of Proopiomelanocortin Neurons in Female Mice. eNeuro. 2018;5(4).
1026 46. Ghamari-Langroudi M, Digby GJ, Sebag JA, Millhauser GL, Palomino R, Matthews R, et al.
1027 G-protein-independent coupling of MC4R to Kir7.1 in hypothalamic neurons. Nature.
1028 2015;520(7545):94-8.
1029 47. Krause WC, Rodriguez R, Gegenhuber B, Matharu N, Rodriguez AN, Padilla-Roger AM, et
1030 al. Oestrogen engages brain MC4R signalling to drive physical activity in female mice. Nature.
1031 2021;599(7883):131-5.
1032 48. Padilla SL, Johnson CW, Barker FD, Patterson MA, Palmiter RD. A Neural Circuit
1033 Underlying the Generation of Hot Flushes. Cell Rep. 2018;24(2):271-7.
1034 49. Dror T, Franks J, Kauffman AS. Analysis of multiple positive feedback paradigms
1035 demonstrates a complete absence of LH surges and GnRH activation in mice lacking kisspeptin
1036 signaling. Biology of reproduction. 2013;88(6):146.

1037 50. Steyn FJ, Wan Y, Clarkson J, Veldhuis JD, Herbison AE, Chen C. Development of a
1038 methodology for and assessment of pulsatile luteinizing hormone secretion in juvenile and
1039 adult male mice. Endocrinology. 2013;154(12):4939-45.
1040 51. Talbi R, Ferrari K, Choi JH, Gerutshang A, McCarthy EA, Dischino D, et al.
1041 Characterization of the Action of Tachykinin Signaling on Pulsatile LH Secretion in Male Mice.
1042 Endocrinology. 2021;162(8).
1043 52. Dave JR, Rubinstein N, Eskay RL. Evidence that b-endorphin binds to specific receptors in
1044 rat peripheral tissues and stimulates the adenylate cyclase-adenosine 3',5'-monophosphate
1045 system. Endocrinology. 1985;117:1389-96.
1046 53. Naulé L, Robert V, Parmentier C, Martini M, Keller M, Cohen-Solal M, et al. Delayed
1047 pubertal onset and prepubertal Kiss1 expression in female mice lacking central oestrogen
1048 receptor beta. Hum Mol Genet. 2015;24(25):7326-38.
1049 54. Pfaffl MW. A new mathematical model for relative quantification in real-time RT-PCR.
1050 Nucleic Acids Res. 2001;29(9):e45.
1051 55. Madisen L, Mao T, Koch H, Zhuo JM, Berenyi A, Fujisawa S, et al. A toolbox of Cre-
1052 dependent optogenetic transgenic mice for light-induced activation and silencing. Nature
1053 Neuroscience. 2012;15(5):793-802.
1054 56. Balthasar N, Coppari R, McMinn J, Liu SM, Lee CE, Tang V, et al. Leptin receptor signaling
1055 in POMC neurons is required for normal body weight homeostasis. Neuron. 2004;42(6):983-91.
1056 57. Padilla SL, Carmody JS, Zeltser LM. Pomc-expressing progenitors give rise to antagonistic
1057 neuronal populations in hypothalamic feeding circuits. Nature Medicine. 2010;16(4):403-5.
1058 58. Bosch MA, Tonsfeldt KJ, Ronnekleiv OK. mRNA expression of ion channels in GnRH
1059 neurons: subtype-specific regulation by 17beta-estradiol. Molecular and cellular endocrinology.
1060 2013;367(1-2):85-97.
1061 59. Qiu J, Nestor CC, Zhang C, Padilla SL, Palmiter RD, Kelly MJ, et al. High-frequency
1062 stimulation-induced peptide release synchronizes arcuate kisspeptin neurons and excites GnRH
1063 neurons. Elife. 2016;5.
1064 60. Stincic TL, Qiu J, Connors AM, Kelly MJ, Ronnekleiv OK. Arcuate and Preoptic Kisspeptin
1065 Neurons Exhibit Differential Projections to Hypothalamic Nuclei and Exert Opposite
1066 Postsynaptic Effects on Hypothalamic Paraventricular and Dorsomedial Nuclei in the Female
1067 Mouse. eNeuro. 2021;8(4).
1068 61. Qiu J, Stincic TL, Bosch MA, Connors AM, Kaech Petrie S, Ronnekleiv OK, et al. Deletion
1069 of Stim1 in Hypothalamic Arcuate Nucleus Kiss1 Neurons Potentiates Synchronous GCaMP
1070 Activity and Protects against Diet-Induced Obesity. The Journal of neuroscience : the official
1071 journal of the Society for Neuroscience. 2021;41(47):9688-701.
1072

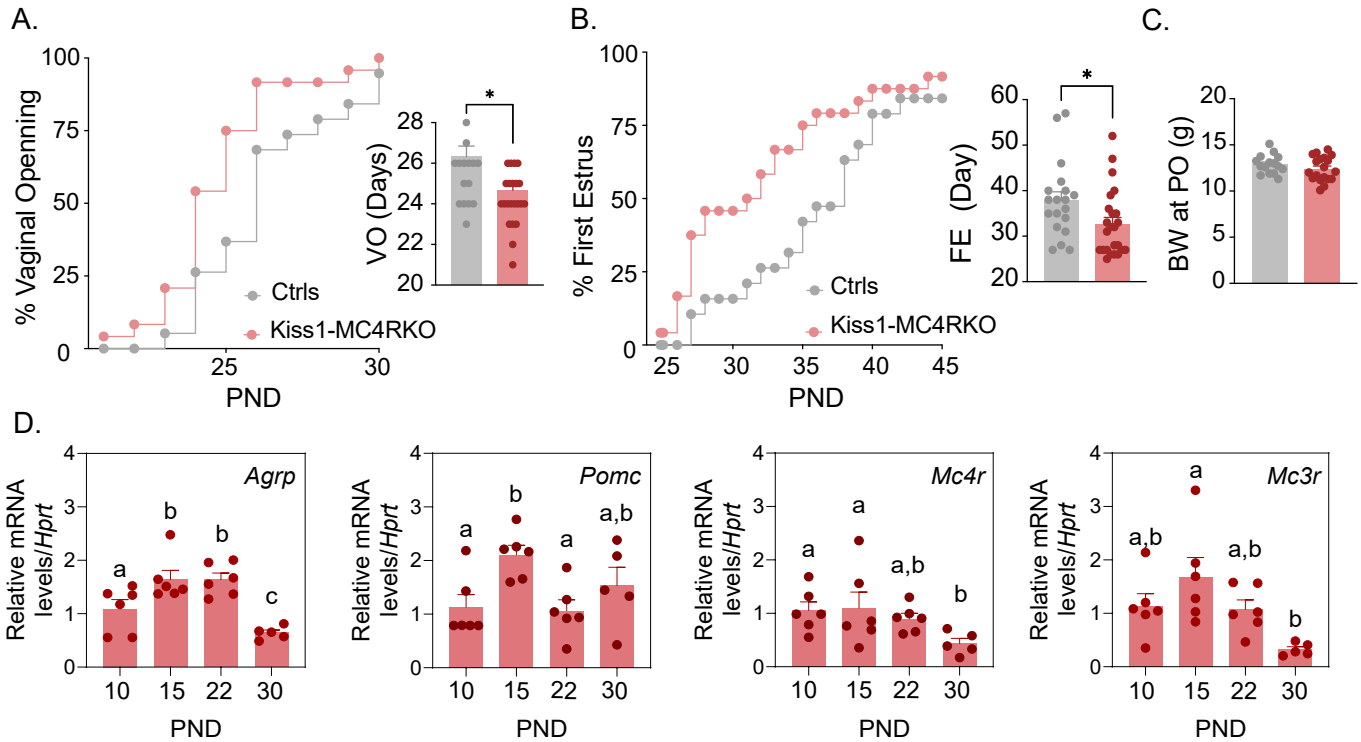
A.
% Vaginal Openning
PND
Ctrls
Kiss1-MC4RKO
VO (Days)
*
B.
% First Estrus
PND
Ctrls
Kiss1-MC4RKO
FE (Day)
*
C.
BW at PO (g)
D.
Relative mRNA levels/Hprt
Agrp
Pomc
Mc4r
Mc3r
PND

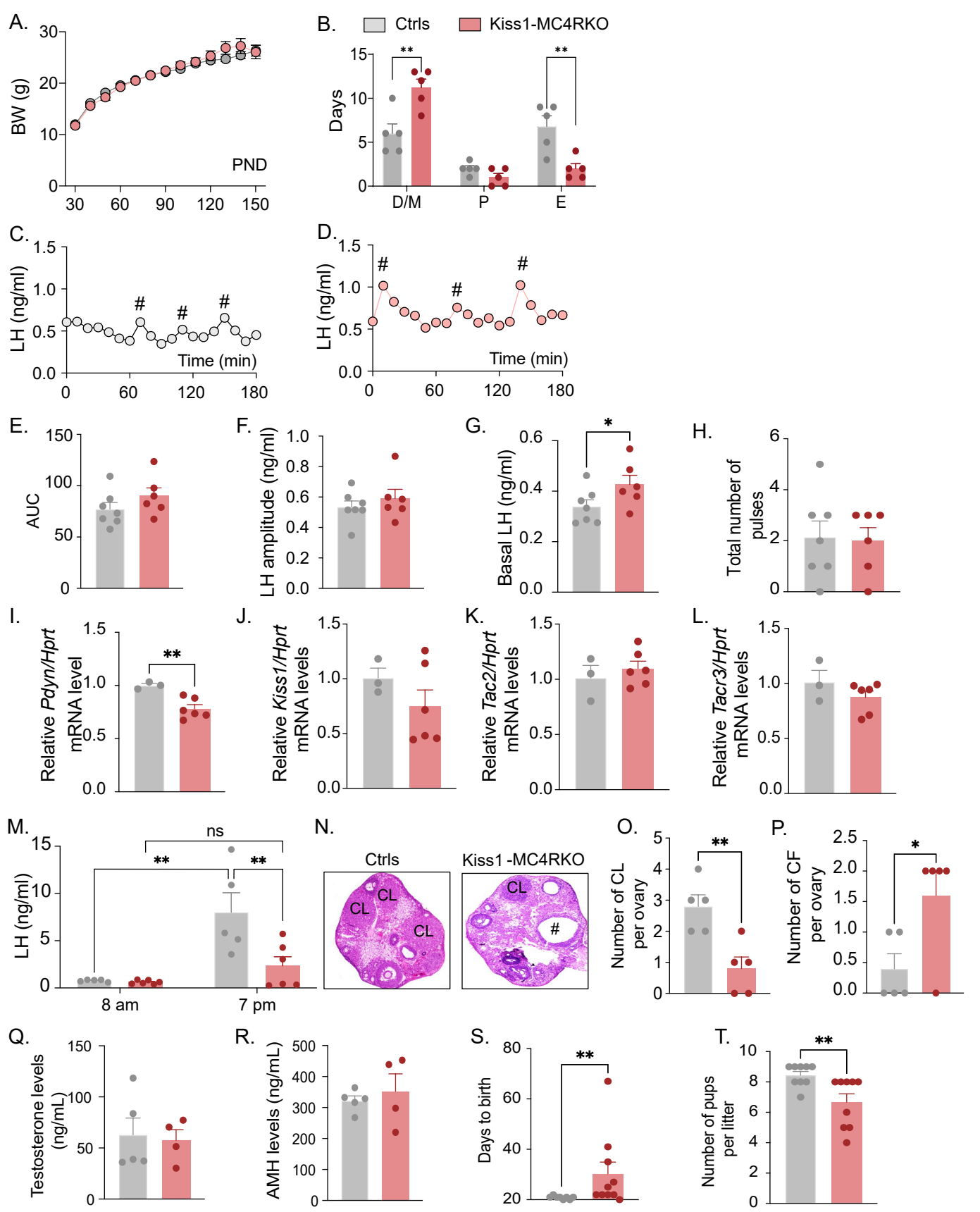
A.
BW (g)
PND
B.
Ctrls
Kiss1-MC4RKO
Days
D/M
P
E
C.
LH (ng/ml)
Time (min)
D.
LH (ng/ml)
Time (min)
E.
AUC
F.
LH amplitude (ng/ml)
G.
Basal LH (ng/ml)
H.
Total number of pulses
I.
Relative Pdyn/Hprt mRNA level
J.
Relative Kiss1/Hprt mRNA levels
K.
Relative Tac2/Hprt mRNA levels
L.
Relative Tacr3/Hprt mRNA levels
M.
LH (ng/ml)
ns
8 am
7 pm
N.
Ctrls
Kiss1 -MC4RKO
CL
O.
Number of CL per ovary
P.
Number of CF per ovary
Q.
Testosterone levels (ng/mL)
R.
AMH levels (ng/mL)
S.
Days to birth
T.
Number of pups per litter

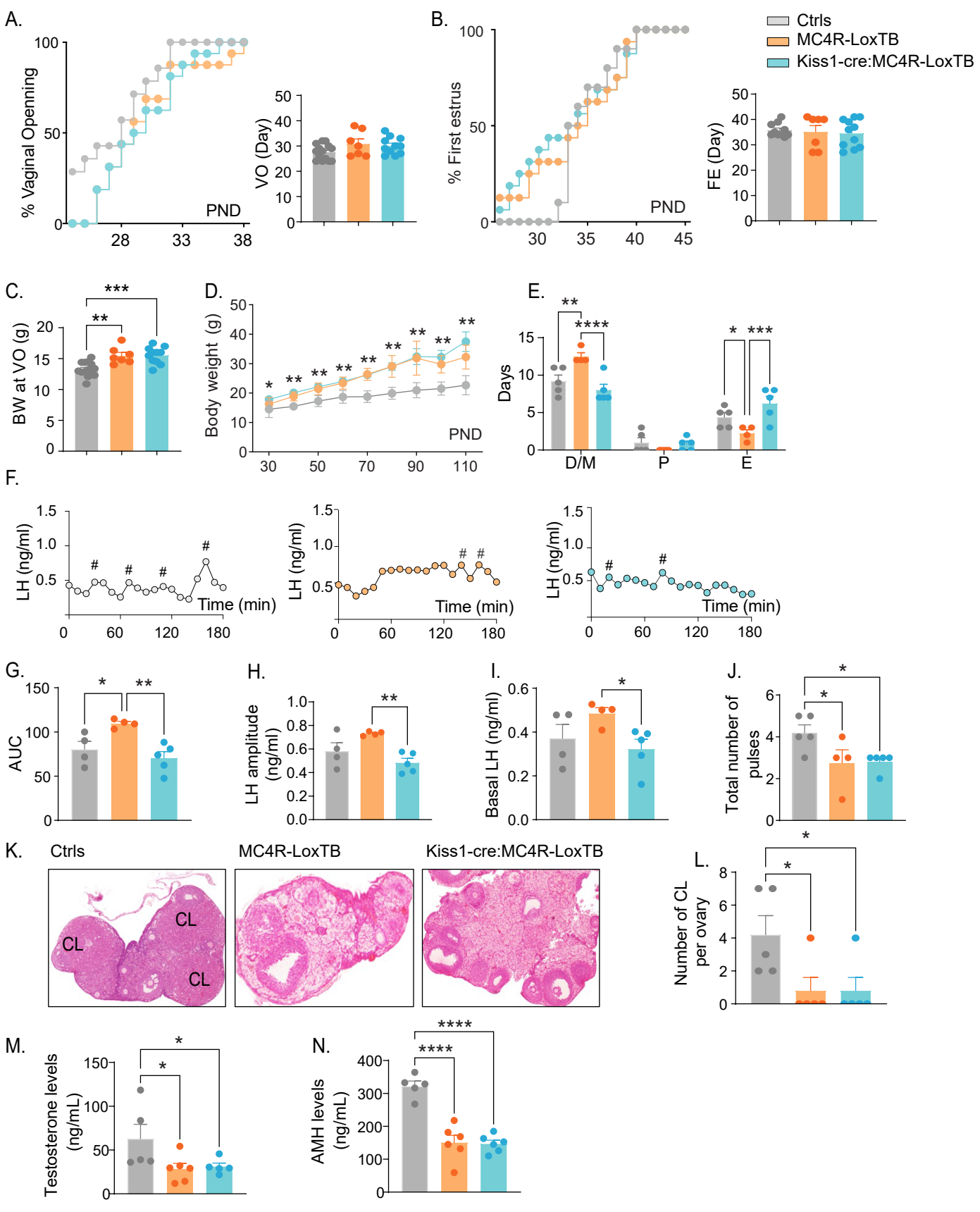
A.
% Vaginal Openning
PND
VO (Day)
B.
% First estrus
PND
FE (Day)
Ctrls
MC4R-LoxTB
Kiss1-cre:MC4R-LoxTB
C.
BW at VO (g)
D.
Body weight (g)
PND
E.
Days
D/M
P
E
F.
LH (ng/ml)
Time (min)
G.
AUC
H.
LH amplitude (ng/ml)
I.
Basal LH (ng/ml)
J.
Total number of pulses
K.
Ctrls
MC4R-LoxTB
Kiss1-cre:MC4R-LoxTB
CL
L.
Number of CL per ovary
M.
Testosterone levels (ng/mL)
N.
AMH levels (ng/mL)

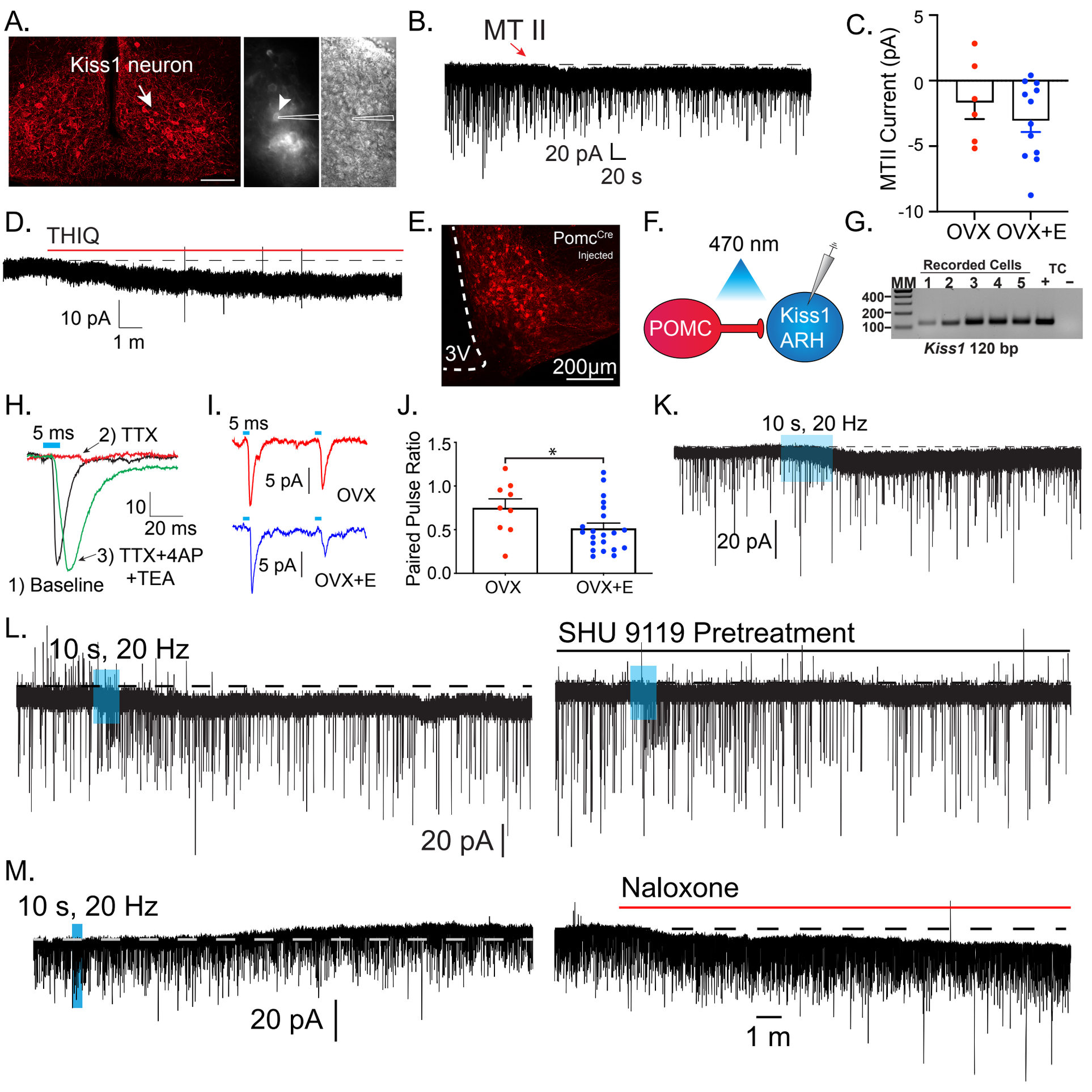
A.
Kiss1 neuron
B.
MT II
20 pA
20 s
C.
MTII Current (pA)
5
0
-5
-10
OVX
OVX+E
D.
THIQ
10 pA
1 m
E.
Pomc^Cre
Injected
3V
200µm
F.
470 nm
POMC
Kiss1
ARH
G.
Recorded Cells
MM
1
2
3
4
5
TC
+
–
400
200
100
Kiss1 120 bp
H.
5 ms
2) TTX
10
20 ms
3) TTX+4AP
+TEA
1) Baseline
I.
5 ms
5 pA
OVX
5 pA
OVX+E
J.
Paired Pulse Ratio
1.5
1.0
0.5
0.0
*
OVX
OVX+E
K.
10 s, 20 Hz
20 pA
L.
10 s, 20 Hz
20 pA
SHU 9119 Pretreatment
M.
10 s, 20 Hz
20 pA
Naloxone
1 m

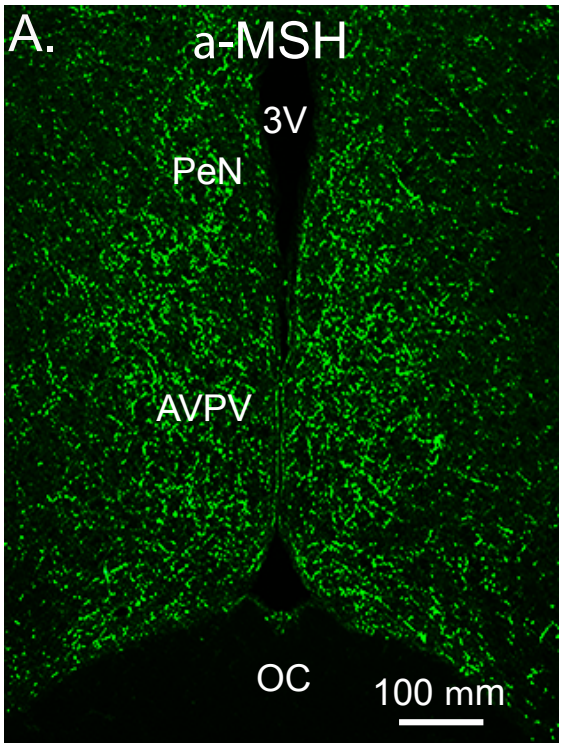
A.
a-MSH
3V
PeN
AVPV
OC
100 mm

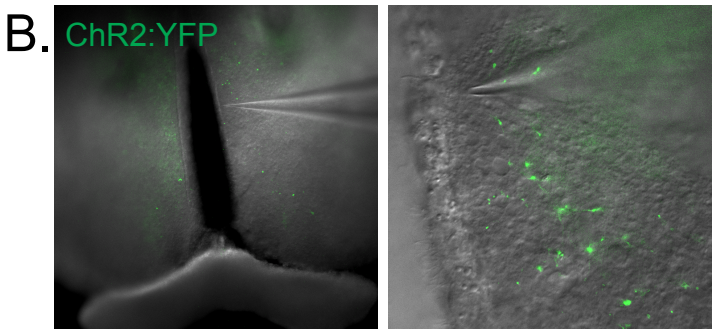
B.
ChR2:YFP

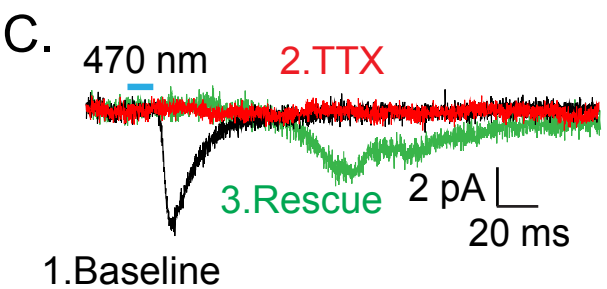
C.
470 nm
2.TTX
3.Rescue
2 pA
20 ms
1.Baseline

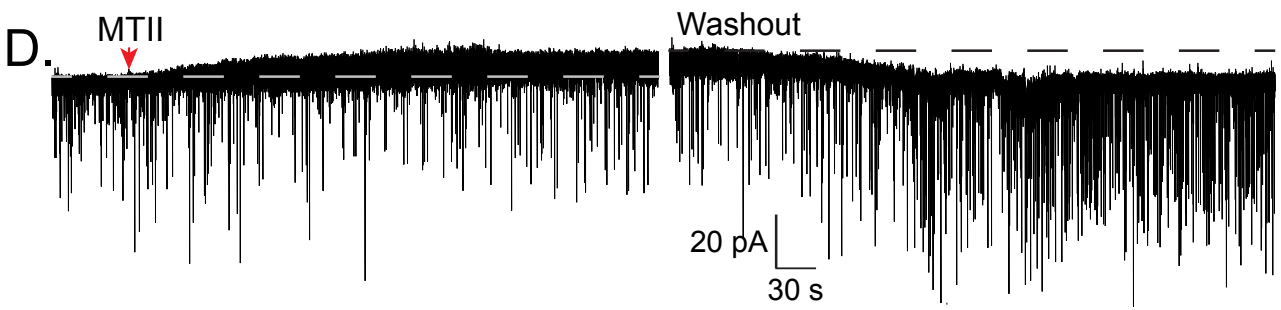
D.
MTII
Washout
20 pA
30 s

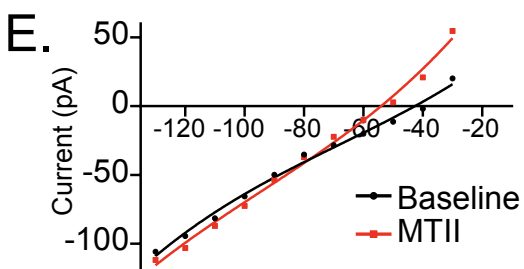
E.
Current (pA)
50
0
-50
-100
-120 -100 -80 -60 -40 -20
Baseline
MTII

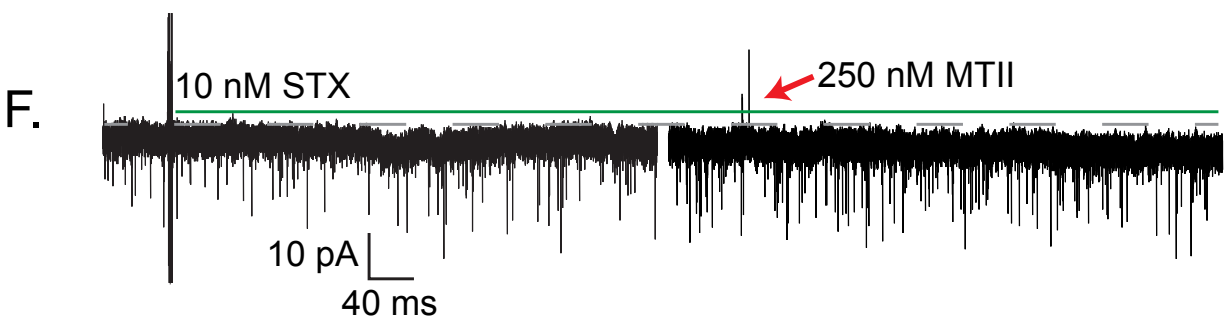
F.
10 nM STX
250 nM MTII
10 pA
40 ms

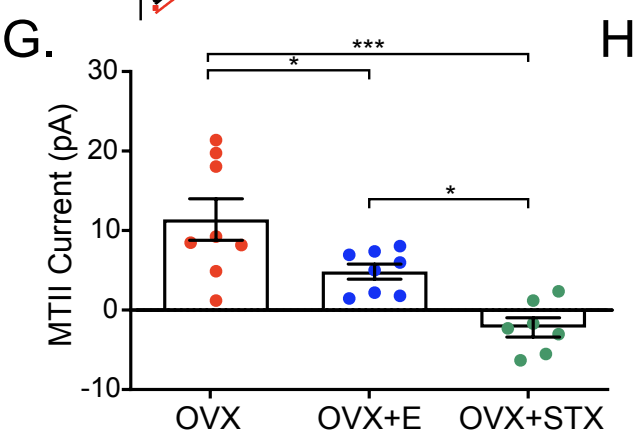
G.
MTII Current (pA)
30
20
10
0
-10
***
*
*
OVX
OVX+E
OVX+STX

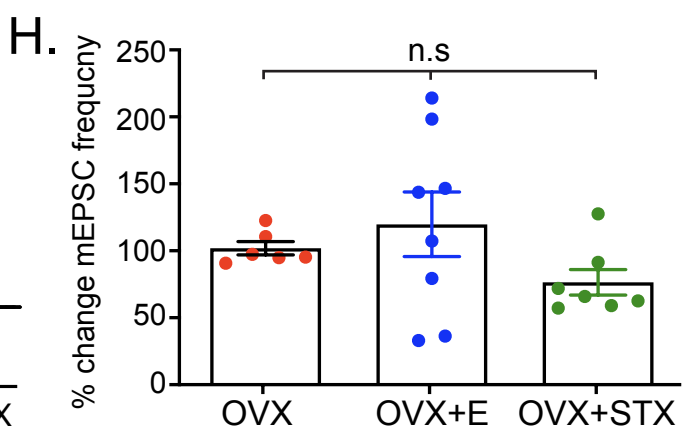
H.
% change mEPSC frequcny
250
200
150
100
50
0
n.s
OVX
OVX+E
OVX+STX

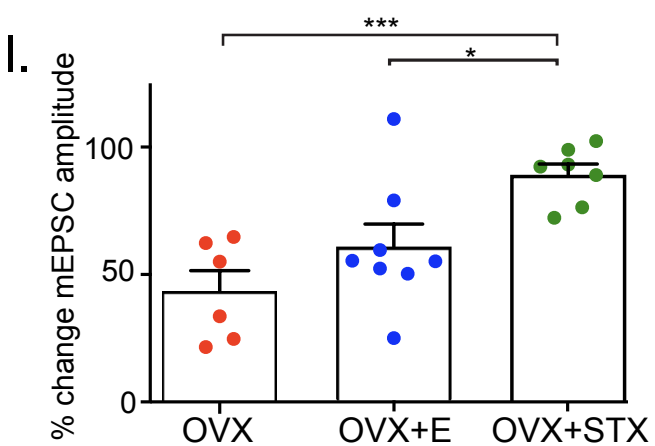
I.
% change mEPSC amplitude
100
50
0
***
*
OVX
OVX+E
OVX+STX

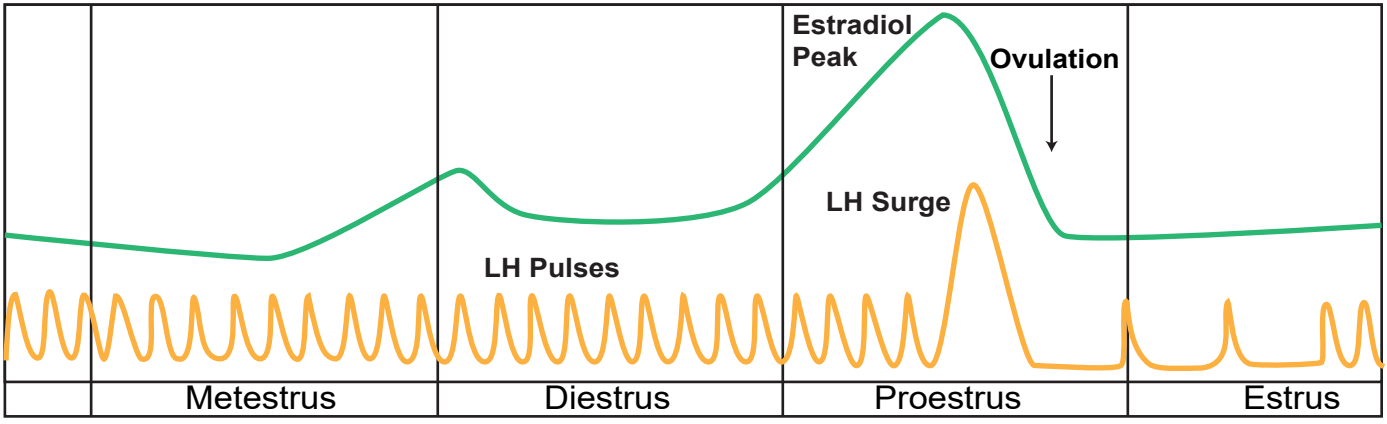
Estradiol
Peak
Ovulation
LH Surge
LH Pulses
Metestrus
Diestrus
Proestrus
Estrus

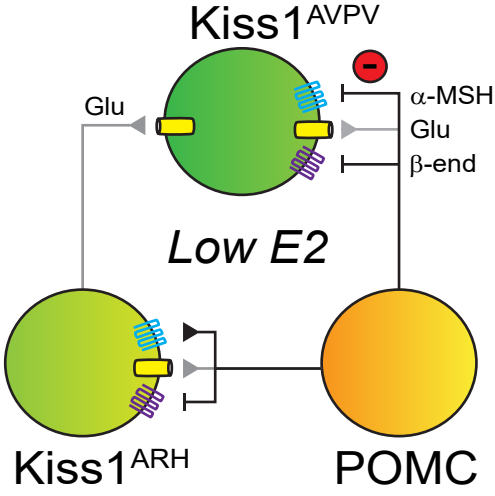
Kiss1AVPV
Glu
α-MSH
Glu
β-end
Low E2
Kiss1ARH
POMC

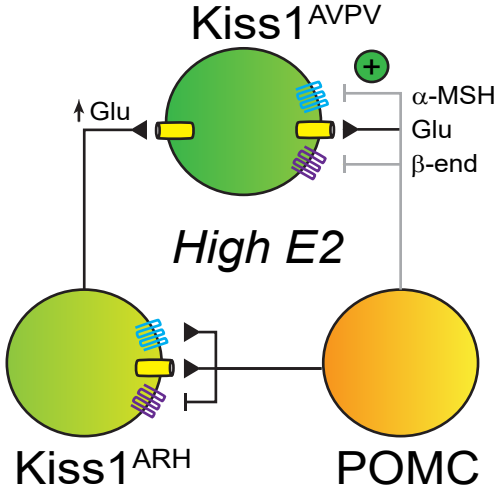
Kiss1AVPV
Glu
α-MSH
Glu
β-end
High E2
Kiss1ARH
POMC